

Stony Brook University



OFFICIAL COPY

The official electronic file of this thesis or dissertation is maintained by the University Libraries on behalf of The Graduate School at Stony Brook University.

© All Rights Reserved by Author.

**STUDIES OF HIGH PRESSURE AND HIGH TEMPERATURE PHYSICAL
PROPERTIES OF LIQUID FeS AND GALLIUM
USING SYNCHROTRON X-RAY**

A Dissertation Presented

by

Tony Yu

to

The Graduate School

in Partial Fulfillment of the

Requirements

for the Degree of

Doctor of Philosophy

in

Geosciences

Stony Brook University

May 2009

Copyright by

Tony Yu

2009

STONY BROOK UNIVERSITY
THE GRADUATE SCHOOL

TONY YU

We, the dissertation committee for the above candidate for the Doctor of Philosophy degree, hereby recommend acceptance of this dissertation.

Jiuhua Chen, Dissertation Advisor
Professor, Mineral Physics Institute, Stony Brook University
Professor, Center for the Study of Matter at Extreme Conditions and
Department of Mechanical and Materials Engineering, Florida International University

Robert Liebermann, Chairperson of Defense
President, Consortium for Materials Properties Research in Earth Sciences
Professor, Department of Geosciences, Stony Brook University

Gilbert Hanson
Professor, Department of Geosciences, Stony Brook University

Brian Phillips
Professor, Department of Geosciences, Stony Brook University

Surendra Saxena
Director and Professor, Center for the Study of Matter at Extreme Conditions, Florida
International University

This dissertation is accepted by the Graduate School.

Lawrence Martin
Dean of the Graduate School

Abstract of the Dissertation

**STUDIES OF HIGH PRESSURE AND HIGH TEMPERATURE PHYSICAL
PROPERTIES OF LIQUID FeS AND GALLIUM
USING SYNCHROTRON X-RAY**

by

Tony Yu

Doctor of Philosophy

in

Geosciences

Stony Brook University

2009

The interior of the earth has always been of great interest to geoscientists. Due to the inaccessibility of samples from deep earth, we have been relying upon other scientific methods and procedures to explore the earth's interior. Cosmochemical and geochemical studies of samples from shallow earth suggest that the core is mainly consisted of Fe, Ni,

and one or more lighter elements. Previous investigations from seismic data and mineral physics data indicate that the outer core's density is about 6% to 10% less than that of pure Fe at the outer core's pressure and temperature conditions, and thus there must be a significant amount of a light element or various kinds of light elements existing in the outer core. The light element candidates in the outer core include C, H, O, S, Si, and the caused density variation might play a critical role in the liquid outer core convection. Using the x-ray absorption radiograph system, we have successfully measured the density of liquid phase FeS at 1673K and up to 5.6GPa in pressure. Our self-developed absorption image fitting program has proved to be reliable in determining the density of liquid FeS. The 15.4 GPa isothermal bulk modulus of liquid FeS at 1673K derived from the density compression curve provides information in constraining the sulfur content in the liquid outer core, which is one of the strong light element candidates that might be responsible for the density deficit in the outer core. To further understand the liquid behavior under extreme condition, we used the pair distribution function (PDF) method to study the structure of an elemental liquid - gallium and its atomic structure change due to compression. Diffuse scattering data were collected over the whole pressure range of liquid state (0.1-2GPa) at ambient temperature. The PDF results show that the first nearest neighbor peak position did not change with pressure increasing, while the farther peaks positions in the intermediate distance range decreased with pressure increasing. This leads to a conclusion of the possible existence of "locally rigid units" in the liquid. With the addition of a series of reverse Monte Carlo modeling of the liquid structure, we

have observed that the coordination number in the local rigid unit increases with pressure. The bulk modulus of liquid gallium derived from the volume compression curve at ambient temperature is 12.1(6) GPa.

Table of Contents

List of Figures	viii
Acknowledgements	xiii
Chapter 1. Introduction	1
Chapter 2. Compressibility of Liquid FeS by Radiograph Imaging	10
2.1. Abstract	10
2.2. Introduction	12
2.3. Experimental Method	14
2.3.1. Radiograph Imaging Method	15
2.3.2. Experimental Setup	19
2.3.3. Absorption Image Analysis	21
2.4. Results and Discussion	23
2.5. References	27
Chapter 3. Pair Distribution Function Study on Compression of Liquid Gallium	41
3.1. Abstract	41
3.2. Introduction	42
3.3. Pair Distribution Function	43

3.4. Experimental Method	45
3.5. Results and Discussion	47
3.6. Atomic Structure Modeling	49
3.7. Summary	52
3.8. References	54
Chapter 4. Exploration for Future Work and Summary	66
4.1. Exploration For Future Work	66
4.1.1. FeS Density Measurement	66
4.1.2. Structural Study	68
4.2. Summary	69
4.3. References	71
References	78

List of Figures

- Figure 2.1 The radiograph system at Beamline X17B2. is an add-on system attached to the in situ x-ray beamline setup. It includes a YAG crystal, an optical mirror, focusing-magnification lenses, and a CCD camera. The monochromatic x-ray beam penetrates through the sample and impinges on the fluorescent screen, where a visible sample image based on the intensity of the transmitted x-ray beam is generated..... 31
- Figure 2.2 Equations and cartoon figures showing the intensity relationship between the penetrated and incident beams. Top: Beam penetrating one homogeneous material. Bottom: Beam penetrating two different materials (sample and reference sphere). R is the density of the material, m is the mass absorption coefficient of the material, and l is the x-ray beam path length inside the sample..... 32
- Figure 2.3 The detailed cell assembly setup for the large volume multi-anvil press experiment is shown in **2.3a**. **2.3b** shows the parameters of the FeS sample and the Al_2O_3 reference sphere that were used in the modified Beer-Lambert Law equation..... 33
- Figure 2.4 Illustration of the DIA-type large volume multi-anvil press used to generate pressure in this experiment..... 34
- Figure 2.5 Radiograph image of the step-absorber consisting of copper foils (**Figure 2.5a**). Comparison of observed brightness and calculated x-ray intensity through the step absorber (**Figure 2.5b**). (Chen *et al.*, 2005)..... 35

Figure 2.6 The relation of the measured brightness and the calculated intensity forms a linear fit ($R^2=0.9999$). (Chen <i>et al.</i> , 2005).....	36
Figure 2.7 A radiograph image recorded by the CCD camera. It clearly shows the corundum reference sphere (bright circle) sitting inside the FeS sample powder (dark area). The square shape outlines the area of data points that we used for density fitting analysis.....	37
Figure 2.8 Brightness (intensity) fitting process improvements. 2.8a is a single slice of the measured sphere image. 2.8b shows the 1-dimensional fitting result using a single slice of the sphere image. 2.8c is the fitted result by applying the lately developed 2-dimensional image fitting method.....	38
Figure 2.9 Isothermal density compression curves from different liquid Fe-Xwt%S alloy studies.....	39
Figure 2.10 The effect of sulfur content on the Fe-Xwt%S alloy isothermal bulk modulus change at 1650K. The figure is modified from the Sanloup <i>et al.</i> , 2000 report. The generated exponential trend line between pure Fe (Fe-0wt%S) (Hixon <i>et al.</i> , 1990) and pure S (Fe-100wt%S) (Tsuchiya, 1994) fits all the data points with $R^2 = 0.9231$. The linear trend line (dotted line) represents ideal mixing of Fe and S and the polynomial trend line (dashed line) shows the atomic fractional bulk moduli of Fe-S alloy that were calculated based on the values from the two end members.....	40
Figure 3.1 The Pair Distribution Function (PDF) provides information of probabilities of finding atom pairs separated by distance r , short-range structure, intermediate-range structure, and average coordination number of the material.....	57

Figure 3.2 Pair distribution function extends the atomic structure study range beyond the first nearest neighbor. Providing structure information of both the first nearest neighbor and intermediate range atomic arrangements.....	58
Figure 3.3 Phase diagram of the element gallium.....	59
Figure 3.4 shows the collected total x-ray scattering patterns of a recrystallized solid phase gallium (Figure 3.4a) and a liquid phase gallium (Figure 3.4b). The characteristic diffraction spots of the solid phase gallium are not observed after reaching the melting point.....	60
Figure 3.5 The normalized $S(Q)$	61
Figure 3.6 From the structure factor of liquid gallium, we see four maximums extending up to $Q=12 \text{ \AA}^{-1}$ from the total elastic scattering by the high energy ($\sim 80\text{KeV}$) synchrotron x-ray. The phase diagram of gallium (Bosio, 1978) shows that the liquid phase exists within the pressure range of 0.1GPa and 2GPa at room temperature. The solid circles show the pressure and temperature condition of the data points acquired for this experiment.....	62
Figure 3.7 The PDF is obtained from the total scattering data via a sine Fourier transform of the normalized scattering intensity $S(Q)$. Therefore, the $G(r)$ shows atomic structure information in real space. The first large peak and its shoulder at 2.78 \AA (#1) and 3.25 \AA (#2) represent the distorted local dense-packed rigid unit. The tail accounts for the intermediate-range correlations. The inset illustrates the peak positions change with pressure. Peak #1 and #2 did not change with pressure but the third peak position decreased by an amount of 0.6%, and the	

fourth peak position decreased 1.5% with pressure increasing. This phenomenon is unusual for compression of hard spheres..... 63

Figure 3.8 The Reverse Monte Carlo modeling result of the experimentally observed $S(Q)$ at 0.27GPa. The total number of atoms applied in the modeling process is 5000. The Reverse Monte Carlo modeling result (open circles) agrees well with the experimental observation (solid line). The coordination number linearly increases with pressure. This reflects the reduction of the distortion of the locally ordered unit..... 64

Figure 3.9 Shown is the fitted 2nd order Birch-Murnaghan equation of state volume compression curve of liquid gallium derived from the RMC modeling result. The calculated isothermal bulk modulus at 300K is 12.1(6) GPa for liquid gallium. For comparison, the triangle shape single data point result is graphically picked from previous ultrasonic measurements study of liquid gallium by Gromnitskaya *et al.* [2007]..... 65

Figure 4.1 shows the image of the gasket and the samples in the diamond anvil cell. Two holes were drilled on the same gasket, each 120 μm in diameter. The left hole was filled with fine Al_2O_3 powder as a sample thickness measurement. The other hole included FeS sample (darker part) surrounded by fine Al_2O_3 powder..... 72

Figure 4.2 The size comparison of the two gasket holes at ambient pressure and under high pressure. The hole that contains the sample (right hand side) was not densely packed as the pure Al_2O_3 powder hole (left hand side). Therefore, the diameter of the sample hole becomes smaller under pressure. A 4GPa difference in pressure between the two chambers was observed by the ruby

scale. The x-ray absorption intensity profile along the yellow line is shown at the very bottom.....	73
Figure 4.3 High pressure and high temperature x-ray total scattering data of liquid gallium has been collected up to 200°C.....	74
Figure 4.4 This figure shows the final PDF G(r) results of liquid gallium collected at ambient temperature (Figure 4.4a), 100°C (Figure 4.4b), and 200°C (Figure 4.4c) at various pressure conditions up to 5.28GPa. The broad but distinctive peaks show where the near-neighbor atoms are located in the local atomic structure. The tail accounts for the medium and long-range correlations. The high temperature G(r)s show similar major features as observed at ambient temperature.....	75
Figure 4.5 The position of Peak #1 remains unchanged at ambient temperature (Figure 4.5a), 100°C (Figure 4.5b), and 200°C (Figure 4.5c). Peak #3 and #4 decrease with pressure. Peak #2 increases at 100°C but decreases at 200°C, showing an inconsistent position change between different temperature conditions. Reason is unclear, but possibly due to the large error that was generated from the poor quality G(r) at 100°C. Further investigation is needed.....	76
Figure 4.6 The calculated interatomic distance change with temperature at 1GPa and 4GPa. Except Peak #2, the 3 other interatomic distances are not affected by temperature within the 200°C temperature range. Temperature has a stronger effect on peak position change at 1GPa.....	77

Acknowledgements

This dissertation was completed with the full support from my advisor Dr. Jiu-hua Chen. I deeply appreciate his encouragement, criticism, and endless patience throughout the research training and the writing of this dissertation. I thank Dr. Michael Vaughan, Dr. Liping Wang, Dr. Zhong Zhong, Dr. Quanzhong Guo, and Dr. Jingzhu Hu, for their tremendous assistance while performing my experiments at the synchrotron beamlines. I have also greatly benefited from discussions with my committee members Dr. Robert Liebermann, Dr. Gilbert Hanson, Dr. Brian Phillips, and Dr. Surendra Saxena. Their precious comments and suggestions have improved the quality of the dissertation.

I am greatly appreciative to all my friends in the Mineral Physics Institute and the Geosciences Department. My research life at Stony Brook was bright and memorable with you around.

I am most grateful to my parents for their doubtless and unconditional support on my research work. For years of countless sacrifices they have made in order to let me pursue my studies 7,700 miles away from home. I thank my wife for her understanding during tough times in research, especially when working stressfully at the beamline. Her strong

support is a major factor for the accomplishment of my research work and this dissertation.

My newborn daughter who arrived 3 days before my scheduled dissertation defense date gave me the final boost of power and strength that I needed to cross the finish line. Thank you, Aneira. Great job!

The Chapter 2 project was supported by NSF research grant EAR-0711321. Use of the National Synchrotron Light Source, Brookhaven National Laboratory, was supported by the U.S. Department of Energy, Office of Science, Office of Basic Energy Sciences, under Contract No. DE-AC02-98CH10886. This research was also partially supported by COMPRES, the Consortium for Materials Properties Research in Earth Sciences under NSF Cooperative Agreement EAR 06-49658. The authors would like to thank Dr. S. Saxena for the helpful discussions and comments, Drs. Z. Zhong, M. Vaughan, L. Wang for their technical support at the beamline.

The work mentioned in Chapter 3 was conducted at the X17B3 beamline of the National Synchrotron Light Source. The use of the NSLS was supported by the U.S. DOE under Contract No. DE-AC02-98CH10886. We would like to thank Dr. Z. Zhong and J. Hu for their support at the beamline. This work is supported by the NSF Grant EAR0711321,

DOE Contract DE-FG02-07E46461, DE-FG02-03ER46085, the COMPRES under NSF

Cooperative Agreement EAR01-35554, and FIU affiliation: Center for the Study of Matter

at Extreme Conditions/ Department of Mechanical and Materials Engineering, Florida

International University, Miami, FL 33199, USA.

Chapter 1

Introduction

The interior of the earth has always been of great interest to geoscientists. Current drilling technique allows us to probe the earth no deeper than 12km from the surface. Due to the inaccessibility of samples from deep earth, we have been relying upon other scientific methods and procedures to explore the earth's interior. Geochemistry and geophysics studies have provided information of the composition and structure of the earth's interior. And based on abrupt changes in physical properties observed by seismic observations, the interior of the earth has been structurally divided into different layers.

Rise of temperature and pressure in the Earth's interior makes the center of the Earth consist of a solid inner core and a liquid outer core. It is believed that the core is responsible for the generation of Earth's magnetic field. Convection of the fluid in the

liquid outer core and its dynamics is therefore crucial for understanding the magnetic field. Due to the high thermal conductivity of the liquid in the outer core, the liquid convection in the outer core has been suggested to be maintained by the chemical composition variation, eg. a buoyancy-driven convection. As a result, the chemical composition and the density of the liquid outer core become critical information in understanding the driven force of the convection.

The outer core that starts at depth 2900 km is still far out of modern mechanical and material technique's reach and its precise composition remains unclear. The only direct detection of the earth's deep interior is via seismic waves. The Preliminary Reference Earth Model (PREM) [Dziewonski and Anderson, 1981] derived from seismic observation has since been the main reference for studying the physical properties of the earth's interior. On the other hand, high pressure and high temperature mineral physics experimental study look at the earth's interior microscopically. Performing precise lab experiments, we simulate the earth in a much smaller scale and with simplified chemical composition in contrast to the real earth condition. Combined with seismic observations, these mineral physics studies help constrain the chemical composition and physical properties of the inaccessible earth interior.

Cosmochemical and geochemical studies of samples from shallow earth suggest that the core is mainly consisted of Fe, Ni, and one or more lighter elements [McDonough, 2003]. Previous investigations from seismic data and mineral physics data indicate that the outer core's density is about 6% to 10% less than that of pure Fe at the

outer core's pressure and temperature conditions [Birch, 1952; McQueen & Marsh, 1966; Jeanloz, 1979; Brett, 1984] and thus there must be a significant amount of a light element or various light elements existing in the outer core [Birch, 1964]. This density variation might play a critical role in the liquid outer core convection. The possible light element candidates that might have significant effect on the density of the core are C, H, O, S, Si [Poirier, 1994; Hillgren *et al.*, 2000]. Among them, sulfur has been suggested as one of the strong candidate due to its abundance, and it plays an important role in the outer core density deficit [Ganapathy and Anders, 1974; Ahrens, 1979; Brown *et al.*, 1984; Ahrens and Jeanloz, 1987]. In order to understand the cause of the density deficit, the density study of liquid phase iron-sulfur alloys (Fe-Xwt%S) will help us constrain the choices of light element candidates and their amount in the liquid outer core.

Density is a material's physical property related to its atomic structure (arrangement). High pressure and high temperature density of a crystalline material can be derived from traditional x-ray Bragg diffraction analysis. However, due to the lack of atomic long-range ordering in non-crystalline materials (ex. glass, liquid), traditional x-ray diffraction is no longer able to tell us the structural/density information of the material. The essential data to establish equation of state of liquid is unobtainable via this widely used detection method. Therefore, other methods to measure liquid density under high pressure and high temperature have been developed. In the case of liquid FeS density measurement, Sanloup *et al.* [2000] determined liquid Fe-Xwt%S (X=10, 20, 27) densities by applying synchrotron x-ray to acquire absorption images. Experiments using

the sink-and-float method with various density markers to determine the density of liquid Fe-Xwt%S alloy have been performed by [Secco *et al.*, 2002; Balog *et al.*, 2003, Nishida *et al.*, 2008]. In our studies, we used monochromatic synchrotron x-ray to collect sample absorption images, and derived the density of liquid FeS by our own developed two-dimensional absorption image intensity fitting program. The bulk modulus of liquid FeS obtained from our measurements was discussed and further combined with other Fe-Xwt%S studies to look at the bulk modulus change of Fe-Xwt%S as a function of sulfur content. We believe this result will be able to serve as a constraint for determining the possible amount of sulfur existing in the liquid outer core.

Possible structure changes with pressure in liquid Fe-S alloys had been reported by others [Morard *et al.*, 2007]. It is therefore necessary to investigate the structure of liquid Fe-S alloys and its change under extreme conditions. The x-ray absorption study of physical properties of liquid FeS under high pressure and high temperature tells us information of the material as a whole. Since non-crystalline materials do not show characteristic Bragg diffraction peaks under x-ray investigation due to their lack of long-range ordering. The structure studies of liquids have therefore been limited, and had been restricted to investigating their local atomic arrangements. In order to understand the local structure of the non-crystalline material and its change with pressure, we have applied total x-ray scattering and pair distribution function (PDF) method to study the local atomic structure and the physical properties of a liquid phase. Information that we can derive from the PDF includes probabilities of finding atom pairs separated by

distance r , short-range structure, intermediate-range structure, and average coordination number of the material. And due to the difficulties of studying the structure of non-crystalline materials using traditional x-ray diffraction technique, the PDF method has become a very important and useful method in liquid structures investigations.

To further understand the liquid structure, a complete structure modeling is required in order to study the material structure in a three-dimensional space. Rietveld refinement is well known for its convenience in analyzing structures of crystalline materials. For structure modeling of disordered materials (liquid, amorphous, etc), the reverse Monte Carlo (RMC) method [McGreevy, 2001] is a powerful and widely accepted modeling method. The structural configurations created from the model helps us understand the structure of disordered material. It also provides information that can help us further determine various physical properties of the study material.

We picked gallium as our PDF study material due to its simple chemical composition and low melting point. The atomic arrangements of liquid gallium and its liquid structure change with pressure were accomplished by a series of Reverse Monte Carlo modeling. This series of gallium PDF and RMC investigation methods can be furthered applied to the structure and physical properties studies of other earth-related materials and topics, especially for those studies that are targeting on liquid phases. For example, studying sulfur as a light element in the outer core. Besides density and physical properties derived from the x-ray absorption method, the liquid phase Fe-S alloy

investigation will greatly benefit from the additional information provided by the PDF and RMC methods.

Chapter 2 is the detailed description of the density measurement and the equation of state study of liquid phase FeS under high pressure and high temperature. The data collection was performed at Beamline X17B at the National Synchrotron Light Source at Brookhaven National Laboratory. The x-ray absorption image analysis program developed by our group [Chen *et al.*, 2005] has been tested and proved to be a reliable method to determine density numbers of liquid phase materials. Designed particularly for our multianvil high pressure and high temperature experimental setup, this program has been applied to this series of density measurement of liquid phase FeS. This chapter, titled *Compressibility of liquid FeS by radiograph imaging* by Yu and Chen is submitted to *Geophysical Research Letters*.

In Chapter 3, I present the work on pair distribution function study and the local atomic structure modeling of liquid phase gallium under pressure. The result is the first part of a series of x-ray total scattering experiments on liquid phase gallium. Since it was the first x-ray total scattering experiment using a diamond anvil cell setup at Beamline X17B at the National Synchrotron Light Source at Brookhaven National Laboratory, it was considered a pioneer experiment at that beamline. The technical development and experimental result titled *High pressure and high temperature pair distribution function study of liquid gallium: clusters in liquid* by Yu, Ehm, Chen, Guo, Luo, and Parise was presented at the 2007 NSLS/CFN User's Meeting and won the Best Poster Award. This

chapter, titled *Pair distribution function study on compression of liquid gallium* by Yu, Ehm, Chen, Guo, Luo, and Parise has been submitted to *Physical Review Letters*.

References

- Dziewonski, A., and D. Anderson, 1981, Preliminary reference Earth model, *Physics of the Earth and Planetary Interiors*, 25, 297-356.
- McDonough, W. F., 2003, in *Treatise on Geochemistry*, ed Carlson R.W., Elsevier, New York, 2, 547-568.
- Birch, F., 1952, Elasticity and constitution of the Earth's interior, *Journal of Geophysical Research*, 57(2), 227-286.
- McQueen, R. G., and S. P. Marsh, 1966, Shock-wave compression of iron-nickel alloys and the Earth's core, *Journal of Geophysical Research*, 71, 1751-1756.
- Jeanloz, R., 1979, Properties of iron at high pressures and the state of the core, *Journal of Geophysical Research*, 84(NB11), 6059-6069.
- Brett, R., 1984, Chemical equilibration of the Earth's core and upper mantle, *Geochimica et Cosmochimica Acta*, 48(6), 1183-1188.
- Birch, F., 1964, Density and composition of mantle and core, *Journal of Geophysical Research*, 69(20), 4377-4388.
- Poirier, J. P., 1994, Light elements in the Earth's outer core- a critical- review, *Physics of the Earth and Planetary Interiors*, 85 (3-4), 319-337.
- Hillgren, V. J., C. K. Gessmann, and J. Li, 2000, An experimental perspective on the light element in Earth's core. In *Origin of the Earth and Moon* (eds. R. M. Canup and K. Righter), 245-263. The University of Arizona Press, Tucson.
- Ganapathy, R. and E. Anders, 1974, Bulk compositions of the Moon and Earth, estimated from meteorites, *Lunar Science V*, Abstracts, Lunar Sci. Inst., Houston, Texas, 254-256.
- Ahrens, T. J., 1979, Equations of state of iron sulfide and constraints on the sulfur content of the Earth, *Journal of Geophysical Research*, 84(B3), 985-998.
- Brown, J. M., T. J. Ahrens, and D. L. Shampine, 1984, Hugoniot data for pyrrhotite and the Earth's core, *Journal of Geophysical Research*, 89, 6041-6048.

- Ahrens, T. J. and R. Jeanloz, 1987, Pyrite: shock compression, isentropic release, and composition of the Earth's core, *Journal of Geophysical Research, B, Solid Earth and Planets*, 92(10), 10,363-10,375.
- Sanloup, C., F. Guyot, P. Gillet, G. Fiquet, M. Mezouar, I. Martinez, 2000, Density measurements of liquid Fe-S alloys at high-pressure, *Geophysical Research Letters*, 27(6), 811-814.
- Secco, R. A., M. D. Rutter, P. S. Balog, H. Liu, D. C. Rubie, T. Uchida, D. Frost, Y. Wang, M. Rivers, S. R. Sutton, 2002, Viscosity and density of Fe-S liquids at high pressures, *J. Phys. Condens. Matter*, 14, 11325-11330.
- Balog, P. S., R. A. Secco, D. C. Rubie, and D. J. Frost, 2003, Equation of state of liquid Fe-10wt%S: Implications for the metallic cores of planetary bodies, *Journal of Geophysical Research*, 108, B2, 2124, ECV 11-1-ECV 11-11.
- Nishida, K., H. Terasaki, E. Ohtani, A. Suzuki, 2008, The effect of sulfur content on density of the liquid Fe-S at high pressure, *Phys. Chem. Minerals*, 35, 417-423.
- Morard, G., C. Sanloup, G. Fiquet, M. Mezouar, N. Rey, R. Poloni, P. Beck, 2007, Structure of eutectic Fe-FeS melts to pressures up to 17 GPa: Implications for planetary cores, *Earth and Planetary Science Letters*, 263, 128-139.
- McGreevy R.L., 2001, Reverse Monte Carlo modeling, *J. Phys. Condens. Matter*, 13, 46, R877-R913.
- Chen, J., D. J. Weidner, L. Wang, M. T. Vaughan, and C. E. Young, 2005, Density measurements of molten materials at high pressure using synchrotron x-ray radiography: Melting volume of FeS, in *Advances in High-Pressure Technology for Geophysical Applications*, Eds. J. Chen, Y. Wang, T.S. Duffy, G. Shen and L.F. Dobrzhinetskaya, ELSEVIER, Amsterdam, pp. 185-194.

Compressibility of liquid FeS by radiograph imaging

2.1. Abstract.

Using the x-ray absorption radiograph system attached to the X17 beamline at the National Synchrotron Light Source at the Brookhaven National Laboratory, we have successfully measured the density of liquid phase FeS at 1673K and up to 5.6GPa in pressure. We applied the second-order Birch-Murnaghan equation of state to calculate the bulk modulus based on our experimentally measured density data. By fixing K' at 4, the 15 (3) GPa isothermal bulk modulus of liquid FeS at 1673K was derived from the density compression curve. This provides information in constraining the sulfur content in the liquid outer core. Combining our bulk modulus

result with those from other Fe-Xwt%S alloys studies we suggest an exponential trend line for the liquid Fe-S alloy bulk modulus change with sulfur content.

2.2. Introduction

Studies of geophysics and geochemistry provide information about the composition and the structure of the Earth's core. Investigations of meteorites reveal that iron makes up bulk of the Earth's core. Meanwhile, seismic observations and mineral physics experimental data indicate that the density of the outer core is about 6% to 10% less than that of pure Fe at the outer core's pressure and temperature conditions (Birch, 1952; McQueen & Marsh, 1966; Jeanloz, 1979; Brett, 1984). The uncertainties in the density deficit are mainly caused by the uncertainties in the estimated core temperature, and also due to the limited experimental studies on the equation of state of iron at high temperatures (Li & Fei, 2003). From the mineral physics point of view, properties of light element-iron alloy are critical for determining the candidate element in the core to account for the density deficit. The density deficit indicates that a significant amount of a light element or a combination of several light elements must exist in the outer core as suggested by Birch (1964). The proposed light element candidates that might have significant effect on the density of the core are C, H, O, S, and Si (Poirier, 1994; Hillgren *et al.*, 2000). Among them, sulfur has been suggested the one relatively abundant, and it plays an important role in the outer core density deficit (Ganapathy and Anders, 1974; Ahrens, 1979; Brown *et al.*, 1984; Ahrens and Jeanloz, 1987). Ahrens (1979) has suggested

that the amount of sulfur in the core is about 9~12wt%. Brown *et al.* (1984) have proposed that the amount of sulfur in the core reaches 10 ± 4 wt%, which is close to the 11 ± 2 wt% result suggested by Ahrens and Jeanloz (1987).

Studies of Fe-S alloys that focused on planetary related problems started in the 70s. A pioneer study was Ahrens' work using the shockwave method to probe the density of natural Fe-S materials (Ahrens, 1979). Brown *et al.* (1984), and Ahrens and Jeanloz (1987) used shockwave as well to study the equation of state of FeS at high pressures and high temperatures. By investigating solid phase FeS, Fei *et al.* in 1995 calculated a liquid state FeS density compression curve at 2173K by applying the thermal pressure based on known parameters from solid state FeS. Although the compression data of the liquid state FeS in Fei *et al.*'s study was not directly from melt density measurements, it presented the first attempt to derive the EOS for FeS melt from static compression. In 2000, Sanloup *et al.* (Sanloup *et al.*, 2000) reported density measurement data of liquid phase Fe-S alloys by applying x-ray absorption techniques. They used the large volume high pressure apparatus and a monochromatic x-ray beam source (58KeV) at the European Synchrotron Radiation Facility (ESRF). The experimental setup includes a sapphire sphere sitting inside the FeS powder as the reference material. They had successfully measured the density of Fe-10wt%S, Fe-20wt%S, and Fe-27wt%S within the pressure range of 1.5-6.2GPa.

The quenched sink-float technique is another popular method used to determine the density of a liquid phase material. Secco *et al.* (2002), Balog *et al.*

(2003), and Nishida *et al.* (2008) measured the density of liquid Fe-Xwt%S alloys in a large volume press. The sink-float technique was applied to their experiments, which they fabricated composite spheres (Pt or WC core + Al₂O₃ mantle) with various densities and placed them in the center of the sample. After the sample melted, the spheres (density markers) with different density numbers showed float, sink, and in some cases, neutral buoyancy behavior caused by the density contrast between the density markers and the liquid phase sample. They were then able to determine the upper and lower density boundary of the liquid material.

Studying the physical properties of liquid phase Fe-Xwt%S (X=0~36) alloys by applying newly developed high pressure and high temperature techniques will help us understand the role of sulfur in the liquid outer core and its impact to the density deficit of the core. The material investigated in this study was FeS (36wt%S). The experiment was conducted using an x-ray radiograph system installed at the National Synchrotron Light Source (NSLS) at Brookhaven National Laboratory (BNL). Density measurement of liquid FeS has been accomplished at 1673K in temperature and at various pressures up to 5.6GPa. We have derived a 4.28g/cm³ zero pressure density and an isothermal bulk modulus of 15 (3) GPa at 1673K for liquid FeS.

2.3. Experimental Method

2.3.1. Radiograph Imaging Method

The radiograph system (Figure 2.1) at Beamline X17B2, NSLS at the Brookhaven National Laboratory is an add-on system attached to the in situ x-ray beamline setup. It includes a YAG crystal as a fluorescent screen, an optical mirror, a long working distance focusing magnification lens, a charge-coupled device (CCD) camera, and a video camera. The monochromatic x-ray beam with energy of 39.7 KeV penetrates through the sample and impinges on the fluorescent screen, where a visible sample image based on the intensity of the transmitted x-ray beam is generated. The contrast of the image is a final result of the density difference, the mass absorption difference, and the thickness difference between the sample and the cell assembly parts. The CCD camera captures the visible image frame by frame, while the video camera can record the image signal continuously. Therefore, the radiograph imaging system setup is capable of recording in situ experimental images under high pressure and high temperature for both static and dynamic experimental conditions.

The x-ray absorption method following the Beer-Lambert Law is applied to this study due to x-ray diffraction method's incapability of detecting structures of liquid phases. When a monochromatic x-ray beam (incident intensity= I_0) passes through a plane-parallel layer of homogeneous, isotropic material of thickness l (cm), with surfaces normal to the beam direction and large enough to cover the total beam

cross-section, the number of ΔI of x-ray photons which are absorbed in a given thickness Δl is proportional to the incident intensity I_0 :

$$-\Delta I \text{ proportional to } I_0 \Delta l \dots\dots\dots(1)$$

The linear absorption coefficient is the fraction of photons absorbed per unit thickness. Equation (1) becomes:

$$-\Delta I = \alpha I_0 \Delta l \dots\dots\dots(2)$$

or

$$-dI = \alpha I_0 dl \dots\dots\dots(3)$$

Integrate Equation (3) from the surface ($l=0$) to a depth l gives the relation of the transmitted x-ray beam intensity $I(l)$ at depth l :

the intensity of the transmitted x-ray beam (I) is:

$$I = I_0 e^{(-\alpha l)} \dots\dots\dots (4)$$

The above equation (Compton & Allison, 1935) defines the linear absorption coefficient α (cm^{-1}) for the primary beam. Since the intensity reduction of the incident beam is determined by the quantity of matter traversed by the primary beam, the thickness of the material penetrated by the beam is often expressed on a mass basis, in gram per square centimeter (g/cm^2), and consequently the mass absorption coefficient α/ρ (cm^2/g) is defined, where ρ (g/cm^3) is the density of the absorption

material. The mass absorption coefficient α/ρ will be presented as μ in the later part of the chapter. Equation (4) may then be written as:

$$I = I_0 e^{-\alpha l} = I_0 e^{-\frac{\alpha}{\rho} \rho l} = I_0 e^{-\mu \rho l} \dots\dots\dots (5)$$

The mass absorption coefficient μ (wavelength dependent) can be calculated from the equations based on atomic descriptions (Henke *et al.*, 1993):

$$\mu = \frac{N_A}{A} \sigma_a \dots\dots\dots (6)$$

$$\sigma_a = 2 \times r_0 \times \lambda \times f_2 \dots\dots\dots (7)$$

- μ : mass absorption coefficient (cm²/g)
- N_A : Avogadro's number
- A : atomic weight (g/atom)
- σ_a : atomic absorption cross section (cm²/atom)
- r_0 : classical electron radius (2.818 × 10⁻¹³ cm)
- λ : wavelength (Angstrom)
- f_2 : atomic scattering factor component (dimensionless)

The Beer-Lambert Law shown in Equation (5) is related to three factors: the mass absorption coefficient of the material μ (cm²/g), the density of the material ρ (g/cm³), and the total travel path length l (cm) that the incident beam penetrates through. By applying this method to the experiment, the density of liquid FeS can be constrained by other known parameters in the equation.

Consider the case where only the material, in this case FeS, with an unknown density is sitting inside the sample chamber. During the experiment, we can measure both the incident and transmitted x-ray beam intensities I and I_0 . μ , the wavelength-

dependent mass absorption coefficient of the material at the specific wavelength is a known parameter. However, under high pressure and temperature the precise dimension of the sample along the beam direction is not measurable. That is, we do not know the total travel length of the x-ray beam inside the material. Therefore generating two unknowns in one equation (Equation 5), one unknown is the x-ray beam travel length inside the sample l , and the other one is the liquid sample density ρ . Relationship between the brightness of the radiograph and the x-ray intensity is presented in Figure 2.2.

To solve this problem, we added a reference material embedded in the sample. A reference material has well known physical properties, for example, the equation of state of the reference material is well known. The simplest and most practical shape of a reference material would be a sphere, as the dimension of a sphere changes continuously in space, and it remains its spherical shape under the experimental pressure and temperature condition. For our specific experimental setup, the sphere sits in the powder sample and the two materials were packed inside a cylindrical sample chamber as shown in Figure 2.3b, the modified Beer-Lambert Law equation in this case is then presented as:

$$B(x, y) = I_0(x, y) K e^{-[\mu_{FeS} \rho_{FeS} (D(x, y) - l(x, y)) + \mu_{Al_2O_3} \rho_{Al_2O_3} l(x, y) + \mu_0 \rho_0 d_0]}$$

$$D(x, y) = 2\left(\left(\frac{D_0}{2}\right)^2 - x^2\right)^{\frac{1}{2}}$$

$$l(x, y) = 2\left[r^2 - (x - x_0)^2 - (y - y_0)^2\right]^{\frac{1}{2}}$$

x & y : coordinates with origin on the cylindrical axis of sample chamber
 x_0 & y_0 : center of the Al_2O_3 sphere
 $B(x,y)$: brightness
 $I_0(x,y)$: x-ray beam intensity before hitting the cell
 K : coefficient of x-ray intensity to radiograph brightness conversion (the radiograph is a 16-bit grayscale image)
 μ : mass absorption coefficient
 ρ : density
 D_0 : diameter of the cylindrical sample chamber
 r : radius of the Al_2O_3 sphere
 d_0 : average x-ray path length in the surrounding materials

For any vertical line penetrating the cell ($x = \text{constant}$):

$$B(x_c, y) = C e^{-[\mu_{\text{FeS}} \rho_{\text{FeS}} (D_c - l(x_c, y)) + \mu_{\text{Al}_2\text{O}_3} \rho_{\text{Al}_2\text{O}_3} l(x_c, y)]}$$

In the equation, μ_{FeS} , $\mu_{\text{Al}_2\text{O}_3}$ can be derived based on the composition of the materials. $\rho_{\text{Al}_2\text{O}_3}$ at a specific pressure and temperature condition is calculated from the thermal equation of state of corundum. ρ_{FeS} can then be acquired by fitting the brightness (intensity of transmitted beam) data across the whole sphere profile into the above equation.

2.3.2. Experimental Setup

Figure 2.3a illustrates the cell assembly of the liquid density measurement experiment. The Al_2O_3 single crystal reference sphere (0.5mm in diameter) was embedded in the center of the FeS powder. Along with a thin cylindrical sodium chloride piece, all the parts were then loaded into the corundum sample chamber. Sodium chloride served as the pressure calibrant following the NaCl equation of

state by Decker (1971). The pressure was generated by SAM85, a DIA-Type large volume multi-anvil press (Figure 2.4). High temperature (1673K) was provided by the graphite cylinder heater, which surrounds the entire sample chamber. The electric power was conducted through platinum wires and foils which have direct contact with the tungsten carbide anvil and the graphite heater. The temperature was measured by a W3%Re-W25%Re type thermal couple. The thermal couple wire tip goes through the cell material, the heater, and then touches the outside wall of the sample chamber. Therefore, provides reading of the sample temperature. No pressure correction was applied to the W-Re thermal couple emf due to the negligible effect. A boron epoxy cube with 6mm edge length was used as the pressure-transmitting medium. The advantage of applying boron epoxy as the pressure medium for holding the sample chamber is that it is transparent to x-ray, which gives us a clear view of the material inside the sample chamber.

The brightness variation on the radiograph image is proportional to the x-ray intensity variation, which was caused by the x-ray absorption difference between the sample and the reference sphere. Therefore, to confirm the linear relation between the brightness of the absorption image and the x-ray intensity is important. Chen *et al.* (2005) demonstrated the good linear correspondence between the x-ray absorption and the x-ray intensity using a step-absorber with identical thickness for each step (Figure 2.5). Figure 2.6 shows the image brightness and x-ray intensity that fit into a straight line ($R^2=0.9999$). The x-ray beam uniformity across the sample will

also affect the accuracy of the experiment. An image of the incident x-ray beam without the sample is collected before the experiment to confirm the intensity uniformity.

Before the melting temperature, the radiograph system yields a maximum 1% difference in measured density comparing with the data collected by the traditional x-ray diffraction method (Chen *et al.*, 2005). X-ray absorption and diffraction data are collected simultaneously, so the disappearance of the diffraction peaks tells us when the sample has turned into liquid phase.

2.3.3. Absorption Image Analysis

Figure 2.7 is a radiograph of the sample chamber acquired by the charge-coupled device (CCD) camera. The radiograph image clearly shows the corundum reference sphere (bright circle) sitting inside the FeS sample powder (dark area). The image is a final result of the monochromatic x-ray beam penetrating through materials with different densities, mass absorption coefficients, and thicknesses (x-ray penetrating path lengths). A square area along the edge of the sphere is then selected out of the full image where we need for brightness fitting and further density analysis.

Previously, the density of the liquid material had been determined by taking a one-dimensional vertical slice of the radiograph. The density is then derived by fitting the brightness curve along the reference sphere. Figure 2.8a shows

a measured brightness from a linear scan across the corundum reference sphere. Figure 2.8b shows both the calculated and the measured brightness curve across the corundum reference sphere. By analyzing several brightness curves at various positions along the sphere, the density of the liquid can be derived. Now, instead of picking a 1-dimensional cross section for the fitting process each time, we have developed a 2-dimensional brightness fitting program (Chen *et al.*, 2005) from the modified Beer-Lambert Law.

A non-linear regression was used to fit the entire reference sphere area in order to determine the melt densities at various temperatures and pressures. An example of the fitting result is shown in Figure 2.8c. The blue points are the measured data, and the red ones are the calculated data points that best fit the observation. This provides a complete coverage of the fitting area taking account of the whole reference sphere, therefore, generating an objective fitting result while comparing with an arbitrary single slice result picked on our own. Another advantage is one can save a lot of time while not having to analyze the data slice by slice but taking care of one whole image at once. However, the tradeoff is a larger density difference between the maximum and the minimum fitted density while analyzing poor quality images, for example, using an imperfectly spherical reference sphere. In this study, the uncertainty of the derived liquid FeS density is statistically estimated to be 2%.

2.4. Results and Discussion

Using an x-ray radiograph system installed at the synchrotron, Stony Brook University has developed an improved in-situ liquid phase density measurement system combined with a large volume press. Chen *et al.* (2005) have used the system to study the melting volume of FeS up to 4GPa and 1573K. This study has reached 5.6GPa in pressure and 1673K in temperature. Combined with our newly developed two-dimensional radiograph brightness fitting method, the uncertainty of the derived liquid FeS density is statistically estimated to be 2%. By applying the second-order Birch-Murnaghan equation of state (Angel, 2000) to fit our density data, we have derived a 4.28g/cm^3 zero pressure density and an isothermal bulk modulus of 15 (3) GPa at 1673K (assuming $K'=4$) for liquid FeS (36wt%S). We have also acquired the FeS liquid density from the same experimental data set by using the old-fashion one-dimensional slice fitting process as described in Chen *et al.*'s (2005) study. We picked 5 vertical slices from the reference sphere along the horizontal direction. The density values were determined by a non-linear regression fitting of the brightness of each slice/curve. The fitted liquid density result compared with the newly developed two-dimensional fitting result is smaller than 1.4%, assuring us the reliability of our new two-dimension image fitting program.

In Figure 2.9, the derived liquid density compression curve is plotted together with results from previous liquid Fe-S alloy studies for comparison purpose. The

liquid FeS (Fe-36wt%S) density derived from this work show lower density values comparing with the Fe-10wt%S liquid density data (Sanloup *et al.*, 2000; Balog *et al.*, 2003) due to the larger sulfur content in FeS. Although the two Fe-10wt%S studies both focused on the same liquid material, there is discrepancy between Balog *et al.*'s (2003) result and Sanloup *et al.*'s (2000), especially at the lower pressure range ($P < 5\text{GPa}$). There is space for improvement of liquid density measurement and our method provides information to constrain the liquid density of Fe-10wt%S at high pressure and high temperature. Also from our study, the FeS composition has a steeper density compression curve slope than the Fe-10wt%S alloy. That is, the lower the sulfur content, the smaller effect pressure has on the density change. To understand the liquid Fe-S alloy density change as a function of pressure and temperature, more information collected from various compositions of Fe-Xwt%S ($X=0\sim 36$), and also from a broader and higher pressure and temperature range is necessary to better constrain the physical properties of liquid Fe-S alloys. We also compared our density result with Nishida *et al.*'s (2008) FeS density result derived from the sink-float method at 4GPa and 1923K. At the same pressure, the calculated density from our density compression curve is 5.13 g/cm^3 . This value is 0.26 g/cm^3 larger than their measured upper limit of liquid FeS density at 1673K, if assuming $dp/dT = 0.0008$ (Nagamori, 1969). The results are comparable considering the estimated 2~3% statistic error from each of these two methods.

From the second-order Birch-Murnaghan equation of state, our study derived an isothermal bulk modulus $K_{0T} = 15$ (3) GPa at 1673K (assuming $K' = 4$) for liquid FeS (Fe-36wt%S). This value is comparable with rough estimation of FeS bulk modulus result (17GPa) that was suggested by Nishida *et al.* (2008). This value falls into the big picture describing the Fe-S alloy bulk modulus (K_{0T}) change with the change of weight percentage of sulfur content at 1650K that was proposed by Sanloup *et al.* in 2000 (Figure 2.10). Based on their liquid density measurements plus other data from previous studies, they have suggested that within the 0~27wt% sulfur content range (0wt%, 10wt%, 20wt%, 27wt% by Hixson *et al.*, 1990 and Sanloup *et al.*, 2000), there is a 2.5GPa decrease in bulk modulus for every 1wt% increase of sulfur in the system at 1650K. This linear relation leads to a negative bulk modulus value after reaching ~32 weight % of sulfur. Our derived bulk modulus for Fe-36wt%S is higher than the projected value that Sanloup *et al.*'s (2000) trend line has predicted. Although the experimental temperature of our data point (1673K) is not exactly the same as the one in Sanloup *et al.*, 2000 (1650K) study, a 23K difference in temperature is believed to have a minor impact on the bulk modulus if assuming that $(\partial K/\partial T)_P$ of the liquid FeS is similar to that of liquid iron (-0.0104 GPa/K) (Hixson *et al.*, 1990). With the addition of liquid FeS bulk modulus derived from this study, here we include the sulfur content of 100 wt% (Tsuchiya, 1994) and fitted available liquid Fe-S alloy bulk moduli experimental data from this study and previous studies. The generated exponential trend line

between pure Fe and pure S fits all the data points with $R^2 = 0.9231$. Assuming the liquid outer core content is Fe mixed with 10wt%S. Then calculated from these two trend lines, the bulk moduli will have a 34.5% (this study) and a 31.3% drop (Sanloup *et al.*, 2000) respectively from pure iron. Also plotted in Figure 2.10 are two trend lines representing ideal mixing of Fe and S (dotted line) and the fractional atomic percentage Fe-S alloy bulk modulus (dashed line) calculated by applying the values from the two end members:

$$K_{\text{Fe-S}} = K_{\text{Fe}} * X_{\text{Fe}} + K_{\text{Sulfur}} * X_{\text{Sulfur}}$$

Where K_{Fe} : pure iron bulk modulus at 1650K (80GPa, Hixon, 1990), K_{Sulfur} : pure sulfur bulk modulus at 673K (1.57GPa, graphically picked from Tsuchiya, 1994), X_{Fe} and X_{Sulfur} : atomic ratio of iron and sulfur in the alloy. Both the ideal mixing trend line and the fractional atomic percentage trend line are quite different from the fitted trend line derived from experimental data, indicating a non-ideal mixing of iron and sulfur in Fe-S alloys. The applied 1.57GPa isothermal bulk modulus of liquid sulfur at 673K (Tsuchiya, 1994) is the highest temperature result that was found in the literature. This value is directly used here as an approximation.

2.5. References

- Ahrens, T. J., 1979, Equations of state of iron sulfide and constraints on the sulfur content of the Earth, *Journal of Geophysical Research*, 84(B3), 985-998.
- Ahrens, T. J. and R. Jeanloz, 1987, Pyrite: shock compression, isentropic release, and composition of the Earth's core, *Journal of Geophysical Research, B, Solid Earth and Planets*, 92(10), 10,363-10,375.
- Angel, R. J., 2000, Equations of state, *High temperature and high pressure crystal chemistry. Reviews in mineralogy and geochemistry*, 41, 35-59.
- Balog, P. S., R. A. Secco, D. C. Rubie, and D. J. Frost, 2003, Equation of state of liquid Fe-10wt%S: Implications for the metallic cores of planetary bodies, *Journal of Geophysical Research*, 108, B2, 2124, ECV 11-1-ECV 11-11.
- Birch, F., 1952, Elasticity and constitution of the Earth's interior, *Journal of Geophysical Research*, 57(2), 227-286.
- Birch, F., 1964, Density and composition of mantle and core, *Journal of Geophysical Research*, 69(20), 4377-4388.
- Brett, R., 1984, Chemical equilibration of the Earth's core and upper mantle, *Geochimica et Cosmochimica Acta*, 48(6), 1183-1188.
- Brown, J. M., T. J. Ahrens, and D. L. Shampine, 1984, Hugoniot data for pyrrhotite and the Earth's core, *Journal of Geophysical Research*, 89, 6041-6048.

- Chen, J., D. J. Weidner, L. Wang, M. T. Vaughan, and C. E. Young, 2005, Density measurements of molten materials at high pressure using synchrotron x-ray radiography: Melting volume of FeS, in *Advances in High-Pressure Technology for Geophysical Applications*, Eds. J. Chen, Y. Wang, T.S. Duffy, G. Shen and L.F. Dobrzhinetskaya, ELSEVIER, Amsterdam, pp. 185-194.
- Compton, A. H. and S. K. Allison, 1935, X-Rays in Theory and Experiment, D. Van Nostrand Company, INC., London, pp. 828.
- Decker, D. L., 1971, High-pressure equation of state for NaCl, KCl and CsCl, *Journal of Applied Physics*, 42, 3239-3244.
- Fei, Y. W., C. T. Prewitt, H. K. Mao, and C. M. Bertka, 1995, Structure and Density of FeS at High Pressure and High Temperature and the Internal Structure of Mars, *Science*, 268(5219), 1892-1894.
- Ganapathy, R. and E. Anders, 1974, Bulk compositions of the Moon and Earth, estimated from meteorites, Lunar Science V, Abstracts, Lunar Sci. Inst., Houston, Texas, 254-256.
- Henke, B. L., E. M. Gullikson, and J. C. Davis, 1993, X-ray interactions: photoabsorption, scattering, transmission, and reflection at $E= 50-30,000$ eV, $Z=1-92$, *Atomic Data and Nuclear Data Tables*, 54, 181-342.
- Hillgren, V. J., C. K. Gessmann, and J. Li, 2000, An experimental perspective on the light element in Earth's core. In *Origin of the Earth and Moon* (eds. R. M. Canup and K. Righter), 245-263. The University of Arizona Press, Tucson.

- Hixson, R. S., M. A. Winkler, M. L. Hodgson, 1990, Sound speed and thermophysical properties of liquid iron and nickel, *Phys. Rev. B*, *42*, 6485-6491.
- Jeanloz, R., 1979, Properties of iron at high pressures and the state of the core, *Journal of Geophysical Research*, *84*(NB11), 6059-6069.
- Li, J. and Y. W. Fei, 2003, Experimental constraints on core composition, *Geochemistry of the Mantle and Core* (ed. R. W. Carlson), 521-546
- McQueen, R. G., and S. P. Marsh, 1966, Shock-wave compression of iron-nickel alloys and the Earth's core, *Journal of Geophysical Research*, *71*, 1751-1756.
- Nagamori, M., 1969, Density of molten Ag-S, Cu-S, and Ni-S systems, *Trans. Metall. Soc. AIME* *245*, 1897-1902.
- Nishida, K., H. Terasaki, E. Ohtani, A. Suzuki, 2008, The effect of sulfur content on density of the liquid Fe-S at high pressure, *Phys. Chem. Minerals*, *35*, 417-423.
- Poirier, J. P., 1994, Light elements in the Earth's outer core- a critical- review, *Physics of the Earth and Planetary Interiors*, *85* (3-4), 319-337.
- Sanloup, C., F. Guyot, P. Gillet, G. Fiquet, M. Mezouar, I. Martinez, 2000, Density measurements of liquid Fe-S alloys at high-pressure, *Geophysical Research Letters*, *27*(6), 811-814.
- Secco, R. A., M. D. Rutter, S. P. Balog, H. Liu, D. C. Rubie, T. Uchida, D. Frost, Y. Wang, M. Rivers, and S. R. Sutton, 2002, Viscosity and density of Fe-S liquids at high pressures, *Journal of Physics: Condensed Matter*, *14*, 11325-11330.

Tsuchiya, Y., 1994, The thermodynamics of structural changes in the liquid sulfur-tellurium system: compressibility and Ehrenfest's relations, *Journal of Physics: Condensed Matter*, 6, 2451-2458.

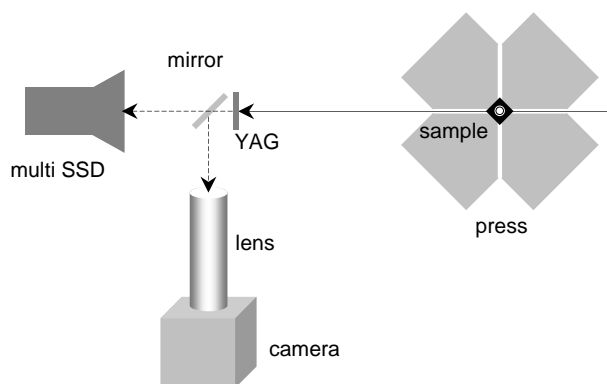


Figure 2.1 The radiograph system at Beamline X17B2. is an add-on system attached to the in situ x-ray beamline setup. It includes a YAG crystal, an optical mirror, focusing-magnification lenses, and a CCD camera. The monochromatic x-ray beam penetrates through the sample and impinges on the fluorescent screen, where a visible sample image based on the intensity of the transmitted x-ray beam is generated.

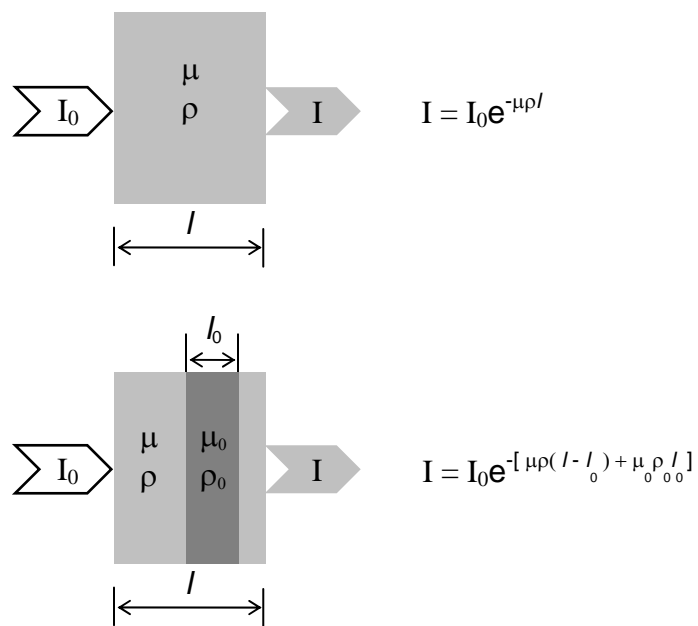


Figure 2.2 Equations and cartoon figures showing the intensity relationship between the penetrated and incident beams. Top: Beam penetrating one homogeneous material. Bottom: Beam penetrating two different materials (sample and reference sphere). ρ is the density of the material, μ is the mass absorption coefficient of the material, and l is the x-ray beam path length inside the sample.

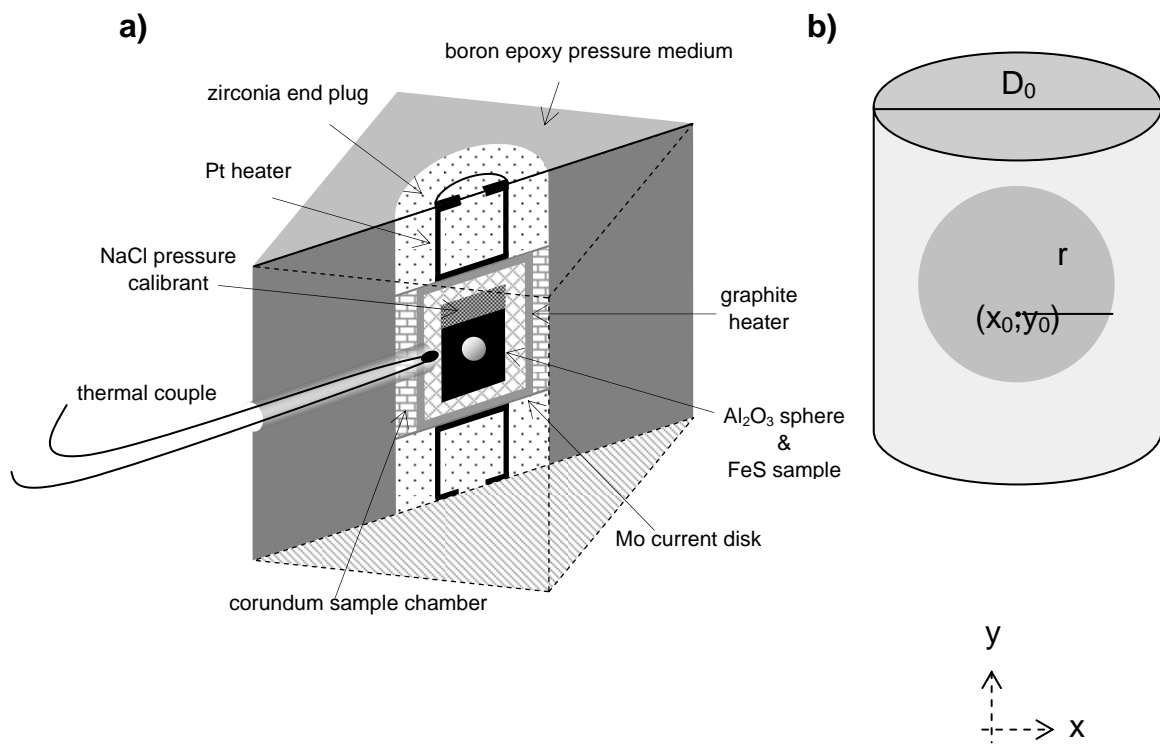
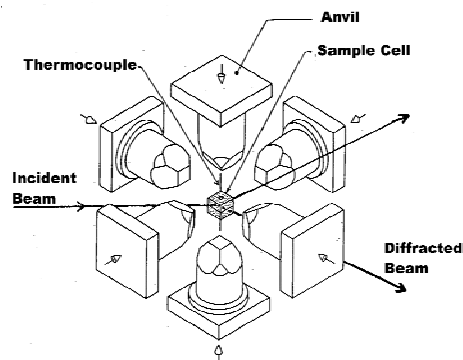
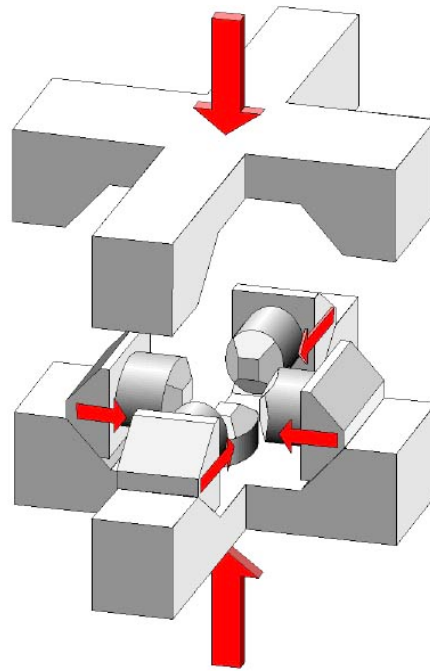


Figure 2.3 The detailed cell assembly setup for the large volume multi-anvil press experiment is shown in **2.3a**. **2.3b** shows the parameters of the FeS sample and the Al₂O₃ reference sphere that were used in the modified Beer-Lambert Law equation.



DIA-type Cubic Anvil Apparatus
"SAM 85"

SAM TEAM:
Jiuhua Chen
Mike Vaughan
Don Weidner

after J. Chen-1/95

Figure 2.4 Illustration of the DIA-type large volume multi-anvil press used to generate pressure in this experiment.

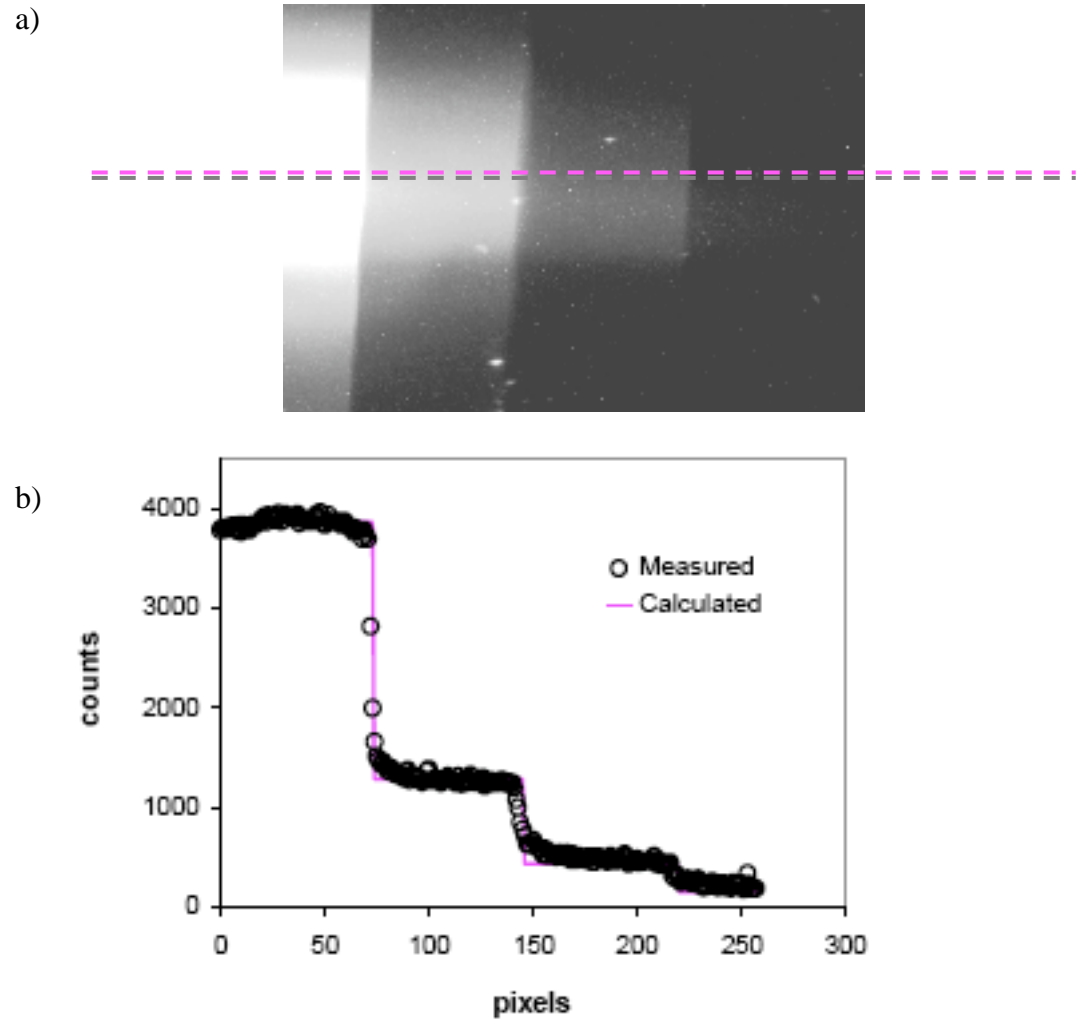


Figure 2.5 Radiograph image of the step-absorber consisting of copper foils (**Figure 2.5a**). Comparison of observed brightness and calculated x-ray intensity through the step absorber (**Figure 2.5b**). (Chen *et al.*, 2005)

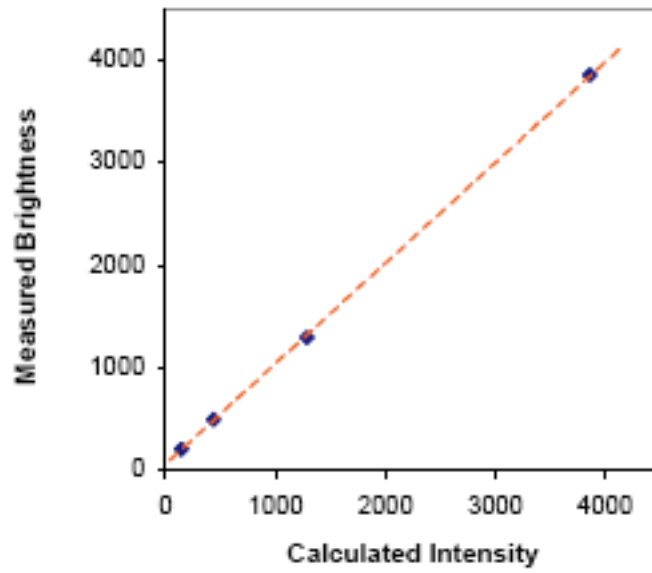


Figure 2.6 The relation of the measured brightness and the calculated intensity forms a linear fit ($R^2=0.9999$). (Chen *et al.*, 2005)

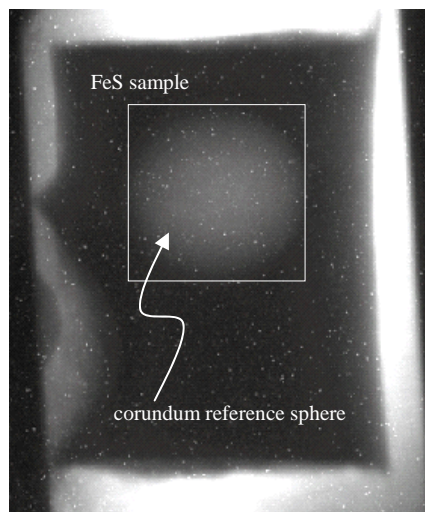


Figure 2.7 A radiograph image recorded by the CCD camera. It clearly shows the corundum reference sphere (bright circle) sitting inside the FeS sample powder (dark area). The square shape outlines the area of data points that we used for density fitting analysis.

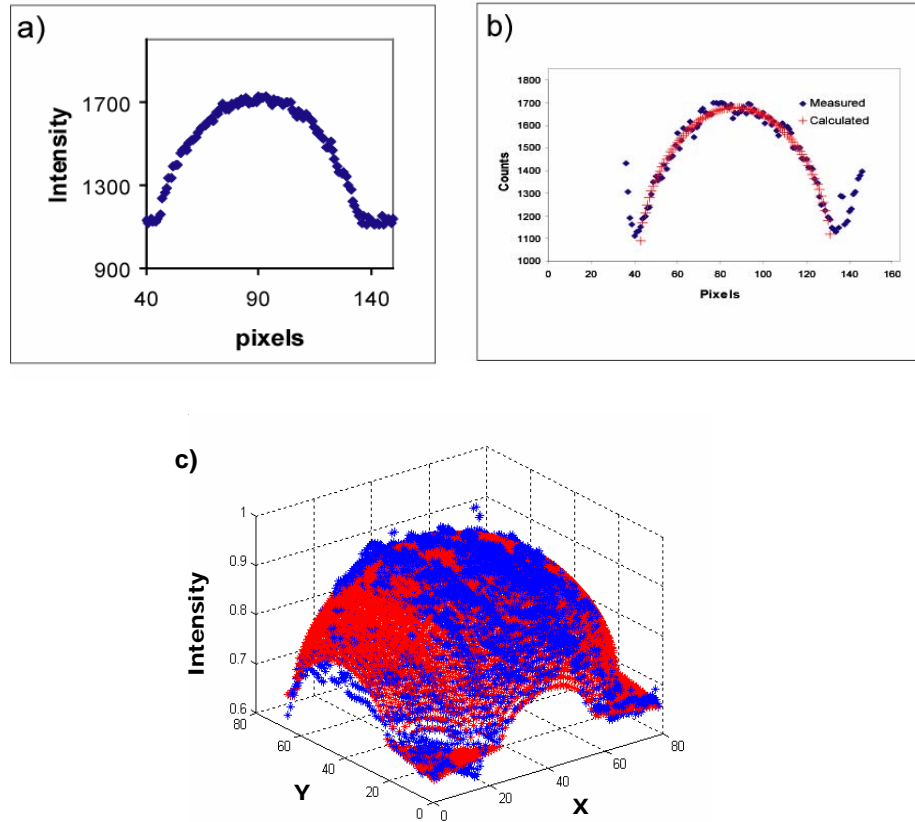


Figure 2.8 Brightness (intensity) fitting process improvements. **2.8a** is a single slice of the measured sphere image. **2.8b** shows the 1-dimensional fitting result using a single slice of the sphere image. **2.8c** is the fitted result by applying the lately developed 2-dimensional image fitting method.

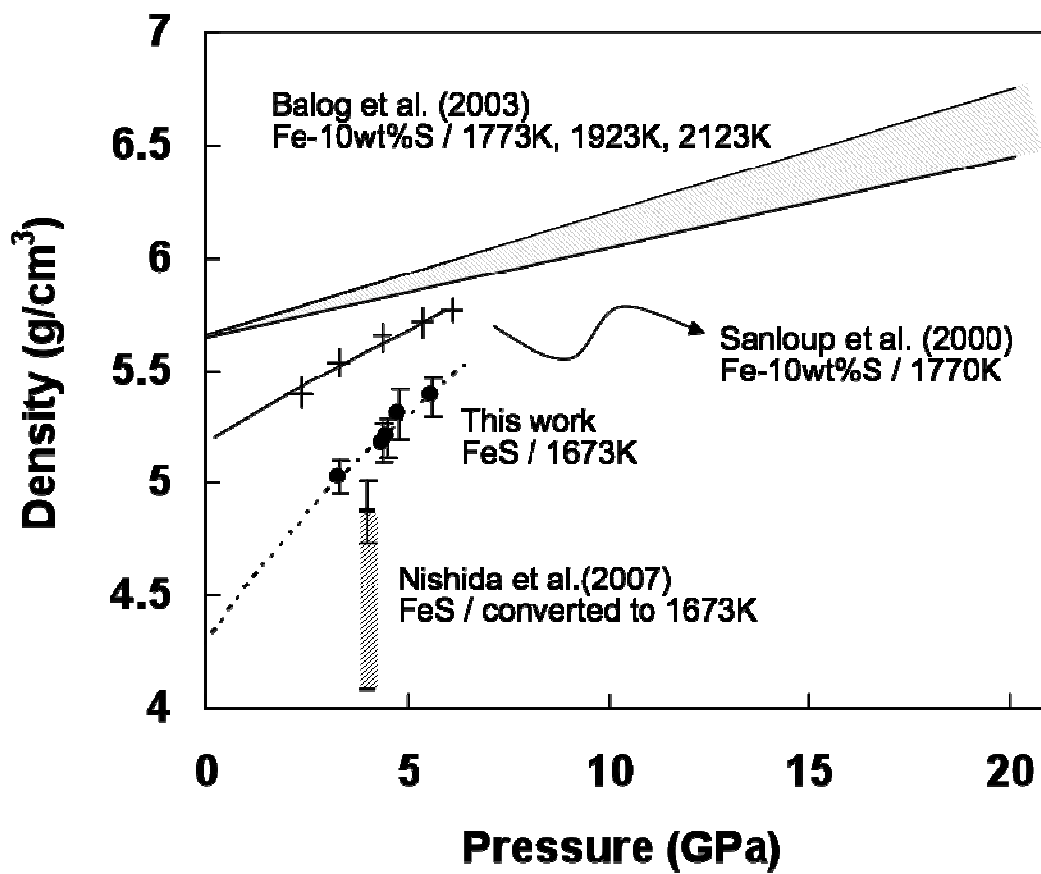


Figure 2.9 Isothermal density compression curves from different liquid Fe-Xwt%S alloy studies.

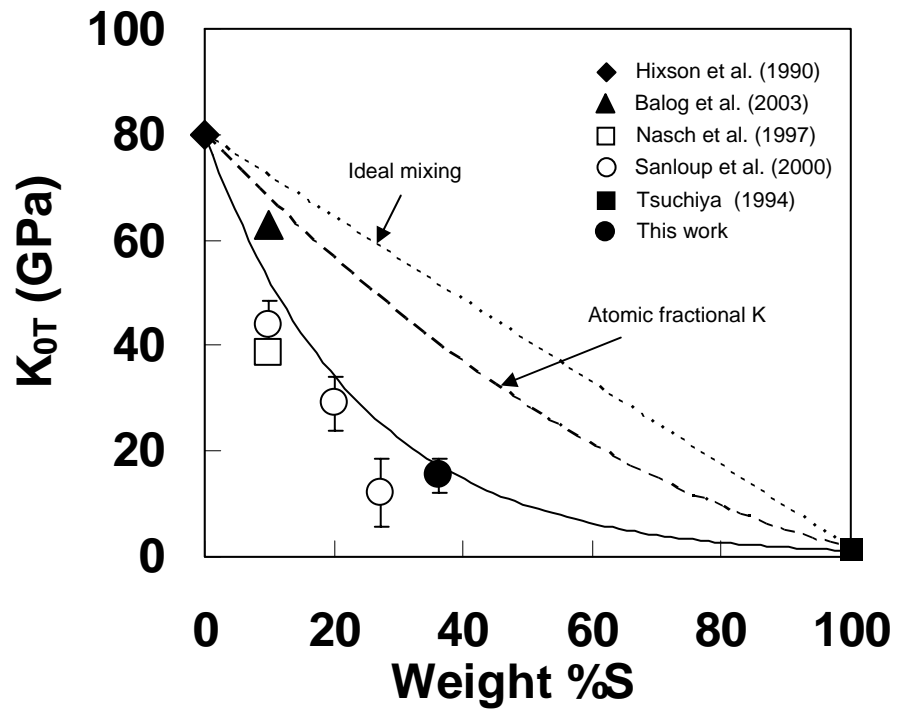


Figure 2.10 The effect of sulfur content on the Fe-Xwt%S alloy isothermal bulk modulus change at 1650K. The figure is modified from the Sanloup *et al.*, 2000 report. The generated exponential trend line between pure Fe (Fe-0wt%S) (Hixon *et al.*, 1990) and pure S (Fe-100wt%S) (Tsuchiya, 1994) fits all the data points with $R^2 = 0.9231$. The linear trend line (dotted line) represents ideal mixing of Fe and S and the polynomial trend line (dashed line) shows the atomic fractional bulk moduli of Fe-S alloy that were calculated based on the values from the two end members.

Pair Distribution Function Study on Compression of Liquid Gallium

3.1 Abstract

Integrating a hydrothermal diamond anvil cell (HDAC) and focused high energy x-ray beam from the superconductor wiggler X17 beamline at the National Synchrotron Light Source (NSLS) at the Brookhaven National Laboratory (BNL), we have successfully collected high quality total x-ray scattering data of liquid gallium. The experiments were conducted at a pressure range from 0.1GPa up to 2GPa at ambient temperature. For the first time, pair distribution functions (PDF) for liquid gallium at high pressure were derived up to 10 Å. Liquid gallium structure has been studied by x-ray absorption [Di Cicco & Filipponi, 1993; Wei *et al.*, 2000; Comez *et al.*, 2001], x-ray

diffraction studies [Waseda & Suzuki, 1972], and molecular dynamics simulation [Tsay, 1993; Hui *et al.*, 2002]. These previous reports have focused on the 1st nearest neighbor structure, which tells us little about the atomic arrangement outside the first shell in non-crystalline materials. This study focuses on the structure of liquid gallium and the atomic structure change due to compression. The PDF results show that the observed atomic distance of the first nearest neighbor at 2.78 Å (first G(r) peak and its shoulder at the higher Q position) is consistent with previous studies by x-ray absorption [2.76 Å, Comez *et al.*, 2001]. We have also observed that the first nearest neighbor peak position did not change with pressure increasing, while the farther peaks positions in the intermediate distance range decreased with pressure increasing. This leads to a conclusion of the possible existence of “locally rigid units” in the liquid. With the addition of reverse Monte Carlo modeling, we have observed that the coordination number in the local rigid unit increases with pressure. The bulk modulus of liquid gallium derived from the volume compression curve at ambient temperature (300K) is 12.1(6) GPa.

3.2 Introduction

Although long-range atomic ordering vanishes in a noncrystalline material, atoms still trend to arrange in an ordered fashion within a few tenths of a nanometer in such materials like liquids and glasses [Waseda, 1980]. Recently, there have been increasingly experimental evidences that liquids may go through first-order transitions under pressure

due to the change of such short range ordering in even elemental melts [Katayama, 1996; Brazhkin, 1997; Glosli, 1999; Tanaka, 2000; Katayama, 2000; Katayama, 2001; Funamori, 2002(a); Funamori, 2002(b); Katayama, 2003]. However, the compression mechanism in liquid state of simple elements is insufficiently studied. Because of lacking the long-range ordering, liquid may reduce its volume in a different way from solid when subject to pressure. For example, compression in solids is always uniform along a given direction (uniform along all directions in an isotropic case). But in liquids, there are a number of elements in the III A, IV A, V A, and VI A groups which do not show uniform compression [Katayama and Tsuji, 2003], i.e. bond length ratio of first nearest neighbors and second nearest neighbors varies as a function of pressure. Here we report a high-energy x-ray diffuse scattering study on liquid gallium (purity 99.999%) at high pressures up to 2 GPa and at a constant temperature of 300 K. The derived liquid gallium pair distribution functions – PDF, $G(r)$, indicate that the distance between the nearest neighbors (the first $G(r)$ peak and a small shoulder peak at high- r side) does not change upon compression whereas distances of higher order nearest neighbors show significant shortening. This observation leads to a speculation of local dense-packed rigid unit (cluster) in the liquid.

3.3 Pair Distribution Function

The Pair Distribution Function (PDF) method is a very powerful tool while helping us investigate atomic structures of non-crystalline material. The information that

we can derive from the PDF (Figure 3.1) includes probabilities of finding atom pairs separated by distance r , short-range structure, intermediate-range structure, and average coordination number of the material. Due to the lack of long range ordered structures in amorphous and liquid materials, it has been difficult to investigate the structure of non-crystalline materials using traditional x-ray diffraction technique. Alternative methods like X-ray absorption (XAS) has been developed and widely used to study the near atomic structure of liquid gallium [Di Cicco & Filipponi, 1993; Wei *et al.*, 2000; Comez *et al.*, 2001a, 2001b]. Their reports have been focused on the 1st nearest neighbor structure, which tell us little about the atomic arrangement outside the first shell in non-crystalline materials. However, with the recent development of the pair distribution functions (PDF) combined with x-ray scattering, we can now study the short to intermediate range structure of a non-crystalline material. Combined with high pressure apparatus, the liquid structure change with pressure can be detected.

According to the equation $Q = 4\pi\sin(\theta)/\lambda$. Where Q is the magnitude of the wave vector, 2θ is the x-ray beam diffraction angle, and λ is the wavelength of the incident x-ray beam. In order to get better quality data of the first peak of the $G(r)$, a greater number in Q is required (observed maximum wavevector Q_{Max}) [Parise *et al.*, 2005]. Plus, for a high quality liquid PDF, a Q_{Max} of at least 10 \AA^{-1} is necessary [Ehm *et al.*, 2007]. There are two ways to increase the Q_{Max} value while setting up the experiment. One is to create a large opening angle on the x-ray beam downstream side of the diamond anvil cell where the x-ray beam exits the sample. In this study, we used a diamond anvil cell with a

$2\theta = 30^\circ$, which gives us a total opening of 60° in front of the area detector. The other way to achieve a high Q_{Max} is to detect the sample using an x-ray beam with a shorter wavelength, that is, higher energy. In this study, the energy of the incident monochromatic x-ray beam was set at 80KeV, which is 0.1549\AA in wavelength. With this particular experimental setup, we were able to reach $Q_{\text{Max}} \sim 20\text{\AA}^{-1}$.

3.4 Experimental Method

The phase diagram of gallium [Bosio, 1978] shows that the liquid phase exists between the pressure range of 0.1GPa and 2GPa at room temperature (29°C) (Figure 3.3). The stable pressure range of the liquid phase widens with the increase of temperature, providing an easily accessible pressure and temperature range for the experimental instruments.

Due to the need of such a high energy x-ray beam, the experiment was conducted using a hydrothermal diamond anvil cell (HDAC) and focused 80keV x-ray beam generated from the superconductor wiggler beamline X17B3 at the National Synchrotron Light Source (NSLS) at the Brookhaven National Laboratory (BNL). The DAC has a 60° opening for diffracted beams, which allows the data collection up to 20\AA^{-1} in Q value ($Q = 4\pi\sin(\theta)/\lambda$). The high energy monochromatic x-ray beam was generated by a bent Laue monochromator, which contains two Si (111) crystals. Two sets of slits (horizontal direction and vertical direction) narrow the incident beam size down to $100\text{ }\mu\text{m}$ by $100\text{ }\mu\text{m}$. The total x-ray scattering signal was collected using a MAR345 image plate detector

(Mar Research). The HDAC was used in the experiment to generate the pressure up to 2GPa. The liquid gallium sample along with a small piece of pressed sodium chloride piece was loaded into the rhenium gasket hole (250 μm in diameter). Sodium chloride acts as the pressure calibrant, it also serves as a standard for determining the sample-to-detector distance and the detector tilt angle correction for the experiment.

Liquid gallium shows very weak x-ray scattering signal. Therefore, to ensure the collection of enough statistics of the weak diffusive scattering signal from the liquid, we collected 20 frames of 5-minute spectra for each data point. The short collection time can also avoid overexposure of Bragg peaks and Compton scattering from the diamond anvils that generates unwanted signal resulting in relatively strong marks in our collected spectrum.

The background signal of the empty HDAC at the experimental temperature was collected before loading the sample. Diffuse scattering data from the liquid gallium at 300K were collected as a function of pressure until it solidifies. Figure 3.4 shows the collected total x-ray scattering patterns of a recrystallized solid phase gallium (Figure 3.4a) and a liquid phase gallium (Figure 3.4b). The characteristic diffraction spots of the solid phase gallium are not observed after reaching the melting point. During the x-ray image processing, the unwanted Bragg peaks shown in the collected patterns that were generated from the diamond anvils were masked off from the images and then integrated by using the fit2d software [Hammersley, 1996, 1997]. The collected x-ray total

scattering patterns were then analyzed by using the software program PDFgetX2 that was developed by Qiu *et al.* [2004] for pair distribution function study.

3.5 Results and Discussion

Figure 3.5 shows an $S(Q)-1$ function after normalization. The normalization process plays a critical part that will affect the results and quality of the pair distribution function $G(r)$. Although the total scattering data was collected up to 20 \AA^{-1} in Q , the data was cut at a Max $Q \sim 13 \text{ \AA}^{-1}$ in order to achieve the best normalization.

Figure 3.6 illustrates the observed structure factors, $S(Q)$, of the collected liquid gallium data at different pressures. Four to five maximums can be recognized in the Q range up to 12 \AA^{-1} . The first $S(Q)$ peak and the shoulder peak at the larger Q value side have also been observed by previous x-ray absorption spectroscopy (XAS) studies [Di Cicco & Filipponi, 1993; Wei *et al.*, 2000; Comez *et al.*, 2001] and x-ray diffraction studies [Waseda & Suzuki, 1972]. However, for the first time, our experiments reveal the higher order of nearest neighbor distance at high pressures. The representative derived $G(r)$ and the change of peak locations of the $G(r)$ as a function of pressure is shown in Figure 3.7. The broad but yet distinctive peaks indicate where the near-neighbor atoms are located in the local atomic structure. The tail accounts for the intermediate-range correlations. The PDF is obtained from the total scattering data via a sine Fourier transform of the normalized scattering intensity $S(Q)$. Therefore, what Figure 3.7 shows

is the information of the atomic structure in real space. The horizontal axis represents the distance between any gallium atom and the center gallium atom, and the vertical axis is the $G(r)$. Comez *et al.* [2001] reported the position of the first $G(r)$ peak at high pressures and discovered that “no detectable distance (position) changes are found”. The liquid gallium first-nearest neighbor distance that we observed at ambient pressure (2.78 Å) is consistent with those reported by Comez *et al.* [2001] and Di Cicco and Filipponi’s [1993], which were determined by x-ray absorption spectroscopy. We also found that within the liquid gallium stable pressure range, this nearest interatomic distance does not change with pressure as illustrated in the Figure 3.7 inset. The same is true for the shoulder peak at 3.25 Å. Nevertheless, the third peak position decreases notably by an amount of 0.6%, and the fourth peak position decreases even more significantly by 1.5% with pressure increasing from 0.27 GPa to 1.97 GPa. This indicates a locally dense-packed rigid unit existing in liquid gallium. Volume reduction due to compression is mainly a result of shortening of bonds beyond the dense-packed unit (i.e. between the third and the fourth nearest neighbors).

Katayama and Tsuji [2003] reviewed the compressions of elemental liquids. They characterized the compression behavior using nearest neighbor distance (r_1/r_1^0) vs. $(V/V_0)^{1/3}$, where V is the molar volume, 0 indicates ambient pressure and $r_1/r_1^0 = (V/V_0)^{1/3}$ represents a uniform compression. They realized that a group of elemental liquids (i.e. alkali metals: Na, K, Rb, Cs) show uniform compressions whereas others (i.e. Ga, Si, Ge, Bi, Se, Te, I) do not. While these liquids deviate from uniform compression in

different ways, Bi shows the same characteristic as Ga that the first nearest neighbor distance is almost constant under pressure. Yaoita *et al.* [1990] attribute this behavior to an increase of coordination number in response to pressure. However, PDF of the gallium liquid shows a very distinct feature that Bi and other liquids do not have: a shoulder peak overlapping with the first $G(r)$ peak at a slightly larger distance, and both peaks do not change their positions with pressure. A simple hard-sphere-like model [Waseda, 1980] cannot fully explain this feature. Tsay [1993] performed a series of molecular-dynamics calculation of liquid gallium structure and gave a structural model ascribing the $S(Q)$ anomalies observed in supercooled gallium liquid or amorphous gallium to the presence of clusters containing different types of atomic bonded pairs (1201-type, 1311-type, and 1301-type). The unchanged interatomic distances features in the compression data for the nearest neighbor distances that was observed in our experiment supports Tsay's cluster concept, that these various atomic bonded pairs may show characteristics of a local dense-packed rigid unit.

3.6 Atomic Structure Modeling

Since liquid or amorphous materials lack periodically long-range atomic arrangement, and due to their disordered nature, to build a unique structure model for liquid or amorphous materials from experimental results or theoretical calculations is almost impossible [Brown *et al.*, 1995]. However, models that correspond to characteristic properties of the liquid are useful for one to understand liquid behaviors.

The pair distribution function provides a one-dimensional picture of the liquid structure. But a complete structure modeling is required in order to study the material structure in a three-dimensional space. Similar to Rietveld refinement in analyzing structures of crystalline materials, for noncrystalline materials (liquid, amorphous, etc), the reverse Monte Carlo (RMC) method [McGreevy, 2001] is a powerful and widely accepted modeling method. The structural configurations created from the model helps us understand the structure of disordered material. It also provides information that can help us further determine various physical properties of the study material. We used the program package WinNFLP to perform the reverse Monte Carlo modeling. We have tried modeling with various numbers of atoms in the system. With too small a number of atoms, we ended up with an unfulfilled fitting result between the RMC model and the experimental observation. Yet, an unreasonably great amount of atoms in the system will take up too much computing power and time in order to run the whole modeling process. An optimized number of atoms (5000) were included in the modeling. The modeling result fits remarkably well with the observed data, as shown in Figure 3.8 for comparison of the calculated (open circles) and the experimentally derived (solid line) structure factor $S(Q)$ at 0.27GPa.

The average coordination number of the liquid structure is derived from the RMC modeling result (Figure 3.8 inset). The value of the coordination number increases as a function of pressure, approaching the coordination number of the center atom in an ideal icosahedron which contains the three types of atomic pairs reported by Tsay [1993]. The

rate of the coordination number increase (6.1% GPa⁻¹) in gallium liquid is less significant than that in Bi liquid (11.4% GPa⁻¹). Therefore, the alternative way for the liquid structure to reflect the volume decrease (density increase) due to compression is to decrease the distances between the local dense-packed rigid units.

The density of liquid gallium at ambient condition that we used as a starting reference for liquid structure modeling is 6.095 g/cm³. This was measured at 29.8°C under room pressure by Hoather [1936]. At high pressure, various density values were applied as input parameters in the RMC modeling. We then calculated the square summation of the intensity difference between the experimental S(Q) and the S(Q) that was generated from the RMC modeling, covering a range from 2 to 11 Å⁻¹. The sample density is determined by finding the least square summation using a 2nd order polynomial fitting of the square summation vs. input density. The error of the derived density at each pressure point is smaller than 1.7%. The S(Q) RMC modeling result shows a 9.9% density increase when the pressure was raised from ambient to 1.97GPa. This density change is greater than that directly estimated using the shortening of the 4th peak (4.4%), indicating that the compression may be accommodated by a combination of inter-cluster distance shortening and coordination number increasing. Using the 2nd order Birch-Murnaghan equation of state (K'=4), we derived the isothermal bulk modulus K=12.1(6) GPa of liquid gallium at 300K. Figure 3.9 illustrates the experimentally observed V/V₀ change with pressure in this study. Also shown in the same figure is a data point graphically picked up from the figure reported by Gromnitskaya *et al.* [2007] at 285K for

comparison. Our data is about 3.3% lower than that by Gromnitskaya *et al.* As no experimental uncertainty of the volume measurement is given in their data, the difference of 3% may be acceptable.

3.7 Summary

High pressure x-ray total scattering experiments in a hydrothermal diamond anvil cell has been performed at Beamline X17B3 at the NSLS. This study was able to detect the local atomic structure of liquid gallium up to 10 Å in distance and valuable information from liquid materials at high pressure has been derived. The physical properties change of liquid gallium under pressure has also been discussed. Based on the experimental observation, existence of atomic locally-ordered-units in liquid gallium is suggested. The possible structure geometry of the locally-ordered-unit may look like a distorted icosahedron with a 10- to 11-gallium-atom-shell surrounding one single gallium atom located inside the distorted icosahedron. There is still space for improvement of the collected data quality. Since the liquid structure is built upon the statistic average of the atom positions, increasing the number of frames collected for each pressure and temperature condition will improve the statistics and give us better quality images. However, this is restricted by the limited assigned beam time at the synchrotron light source. Applying perforated diamonds will reduce the relatively strong bright spots in the images generated by Bragg peaks of the single crystal diamond anvils. Or we could

prevent the unwanted bright spots by physically blocking the scattering signal in front of the detector by applying small lead pieces on the imaging plate surface.

3.8 References

- Bosio, L., 1978, Crystal structures of Ga(II) and Ga(III), *J. Chem. Phys.*, 68, 1221-1223.
- Brazhkin, V. V., S. V. Popova, R. N. Voloshin, 1997, High-pressure transformations in simple melts, *High Pressure Research*, 15, 267-305.
- Brown, Jr., G. E., F. Farges, G. Calas, 1995, X-ray scattering and x-ray spectroscopy studies of silicate melts, *Reviews in Mineralogy*, 32, 317-410.
- Comez, L., A. Di Cicco, J. P. Itie, and A. Polian, 2001, High-pressure and high-temperature x-ray absorption study of liquid and solid gallium, *Physical Review B*, 65, 014114-1-014114-10.
- Comez, L., A. Di Cicco, M. Minicucci, R. Tossici, J. P. Itie, and A. Polian, 2001, EXAFS study on liquid gallium under high pressure and high temperature, *J. Synchrotron Rad.*, 8, 776-778.
- Di Cicco, A. and A. Filipponi, 1993, Three-body distribution function in liquids: the case of liquid gallium, *J. Non-Cryst. Sol.*, 156-158, 102-106.
- Ehm, L., S. M. Antao, J. Chen, D. R. Locke, F. M. Michel, C. D. Martin, T. Yu, J. B. Parise, P. L. Lee, P. J. Chupas, S. D. Shastri, Q. Guo, 2007, Studies of local and intermediate range structure in crystalline and amorphous materials at high pressure using high-energy x-rays, *Powder Diffraction*, 22 (2), 108-112.
- Funamuri, N., K. Tsuji, 2002, Pressure induced structural change in liquid silicon, *Physical Review Letters*, 88(25), 255508-1-255508-4.
- Funamuri, N., K. Tsuji, 2002, Structural transformation of liquid tellurium at high pressures and temperatures, *Physical Review B*, 65(1), 014105-1-014105-5.
- Glosli, J. N., F. H. Ree, 1999, Liquid-liquid phase transformation in carbon, *Physical Review Letters*, 82 (23), 4659-4662.
- Gromnitskaya, E.L., O. F. Yagafarov, O. V. Stagorova, V. V. Brazhkin, A. G. Lyapin, 2007, Pressure-driven “molecular metal” to “atomic metal” transition in crystalline Ga, *Physical Review Letters*, 98, 165503.

- Hammersley, A. P., S. O. Svensson, M. Hanfland, A. N. Fitch, D. Hausermann, 1996, Two-dimensional detector software: From real detector to idealized image or two-theta scan, *High Pressure Research*, 14, 235-248.
- Hammersley, A. P., 1997, FIT2D: An introduction and overview, ESRF Internal Report, ESRF97HA02T.
- Hoather, W. H., 1936, The density and coefficient of expansion of liquid gallium over a wide range of temperature, *Proceedings of the Physical Society*, 48, 5, 699-707.
- Hui, L., G. Wang, J. Zhao, X. Bian, 2002, Cluster structure and dynamics of liquid aluminum under cooling conditions, *J. Chem. Phys.*, 116, 10809-10815.
- Katayama, Y., K. Tsuji, H. Kanda, H. Nosaka, K. Yaoita, T. Kikegawa, O. Shimomura, 1996, Density of liquid tellurium under pressure, *Journal of Non-crystalline Solids*, 207, 451-454.
- Katayama, Y., T. Mizutani, W. Utsumi, O. Shimomura, M. Yamakata, K. Funakoshi, 2000, A first-order liquid-liquid phase transition in phosphorus, *Nature*, 403(6766), 170-173.
- Katayama, Y., T. Mizutani, W. Utsumi, O. Shimomura, K. Tsuji, 2001, X-ray diffraction study on structural change in liquid selenium under high pressure, *Physica Status Solidi (b)*, 223, 401-404.
- Katayama, Y., Y. Inamura, 2003, Synchrotron radiation studies on pressure-induced structural changes in liquids and glasses, *Journal of Physics: Condensed Matter*, 15(1), S343-S350.
- Katayama, Y., K. Tsuji, 2003, X-ray structural studies on elemental liquids under high pressures, *J. Phys. Condens. Matter*, 15, 23, 6085-6103.
- McGreevy, R.L., 2001, Reverse Monte Carlo modeling, *J. Phys. Condens. Matter*, 13, 46, R877-R913.
- Parise, J. B., S. M. Antao, F. M. Michel, C. D. Martin, P. J. Chupas, S. D. Shastri, and P. L. Lee, 2005, Quantitative high-pressure pair distribution function analysis, *J. Synchrotron Rad.*, 12, 554-559.

- Proffen, Th. and S. J. L. Billinge, 1999, PDFFIT, a program for full profile structural refinement of the atomic pair distribution function, *J. Appl. Cryst.*, 32, 572-575.
- Qiu, X., J. W. Thompson, and S. J. L. Billinge, 2004, PDFgetX2: A GUI driven program to obtain the pair distribution function from X-ray powder diffraction data, *J. Appl. Cryst.*, 37, 678-678.
- Tanaka, H., 2000, General view of a liquid-liquid phase transition, *Physical Review E*, 62 (5), 6968-6976.
- Tsay, S. F., 1993, Structure of rapidly quenched Ga metal, *Phys. Rev. B*, 48, 5945-5948.
- Waseda, Y. and K. Suzuki, 1972, Structure factor and atomic distribution in liquid metals by x-ray diffraction, *Phys. Stat. Sol. B*, 49, 339-347.
- Waseda, Y., 1980, *The Structure of Non-Crystalline Materials*, New York, McGraw-Hill.
- Wei, S., H. Oyanagi, W. Liu, T. Hu, S. Yin, G. Bian, 2000, Local structure of liquid gallium studied by x-ray absorption fine structure, *J. Non-Cryst. Sol.*, 275, 160-168.
- Yaoita, K., K. Tsuji, M. Imai, T. Kikegawa, O. Shimomura, 1990, Structure of liquid bismuth under high pressure, *High Pressure Research*, 4 (1), 339-341.

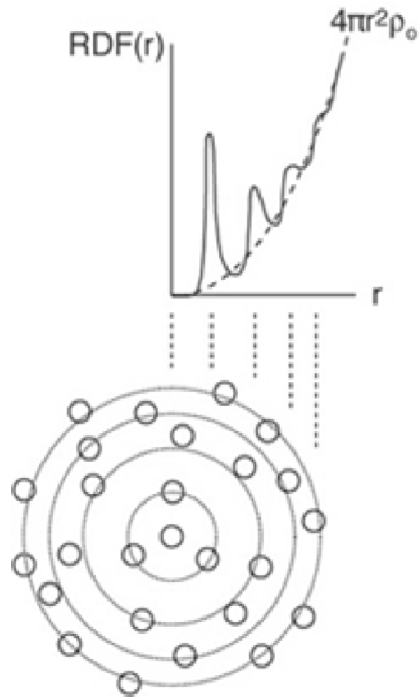


Figure 3.1 The Pair Distribution Function (PDF) provides information of probabilities of finding atom pairs separated by distance r , short-range structure, intermediate-range structure, and average coordination number of the material.

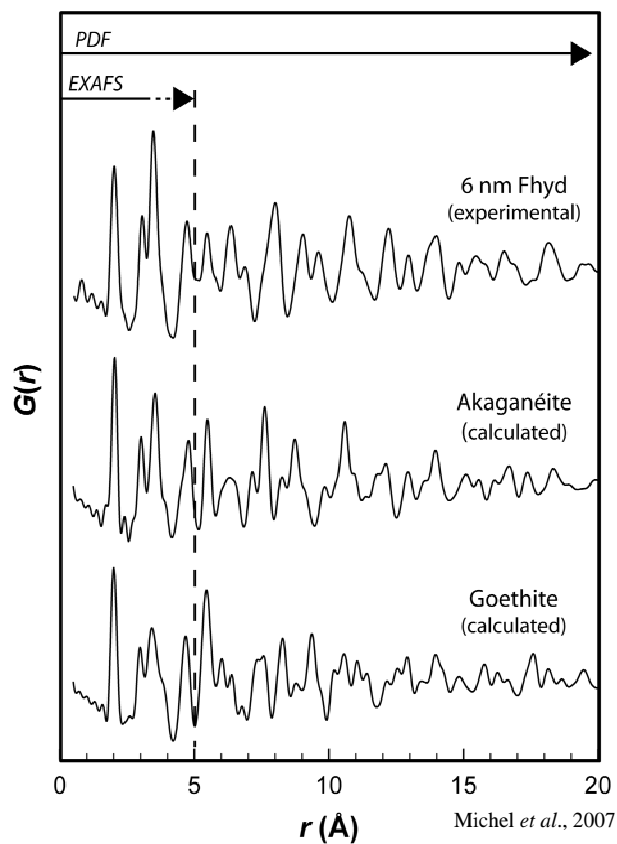


Figure 3.2 Pair distribution function extends the atomic structure study range beyond the first nearest neighbor. Providing structure information of both the first nearest neighbor and intermediate range atomic arrangements.

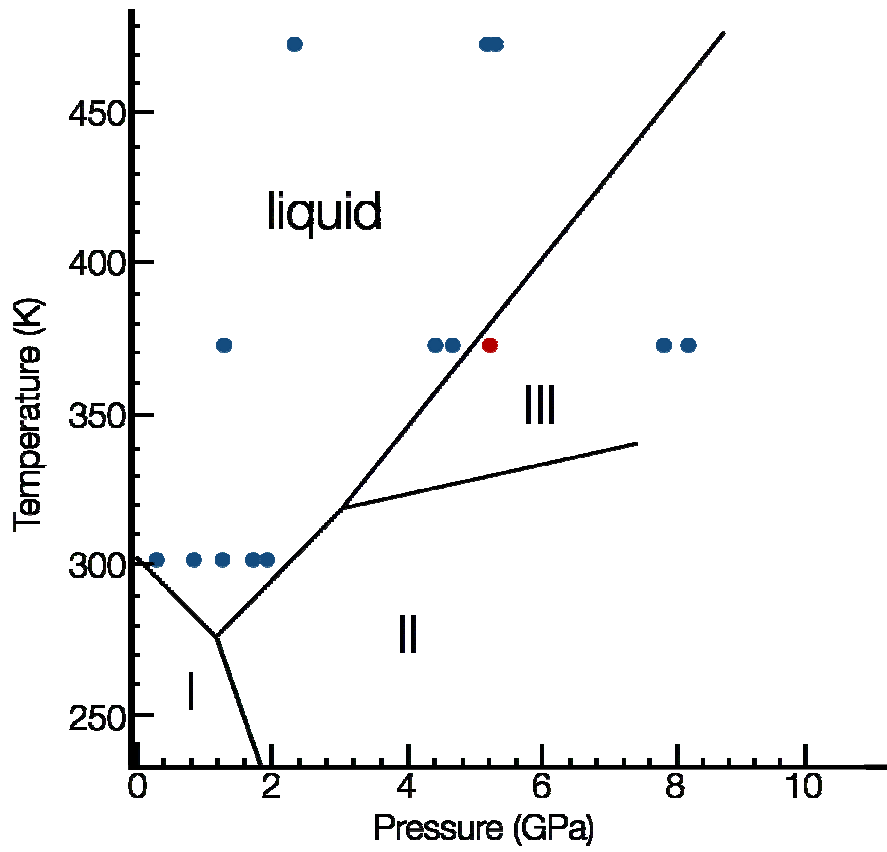


Figure 3.3 Phase diagram of the element gallium

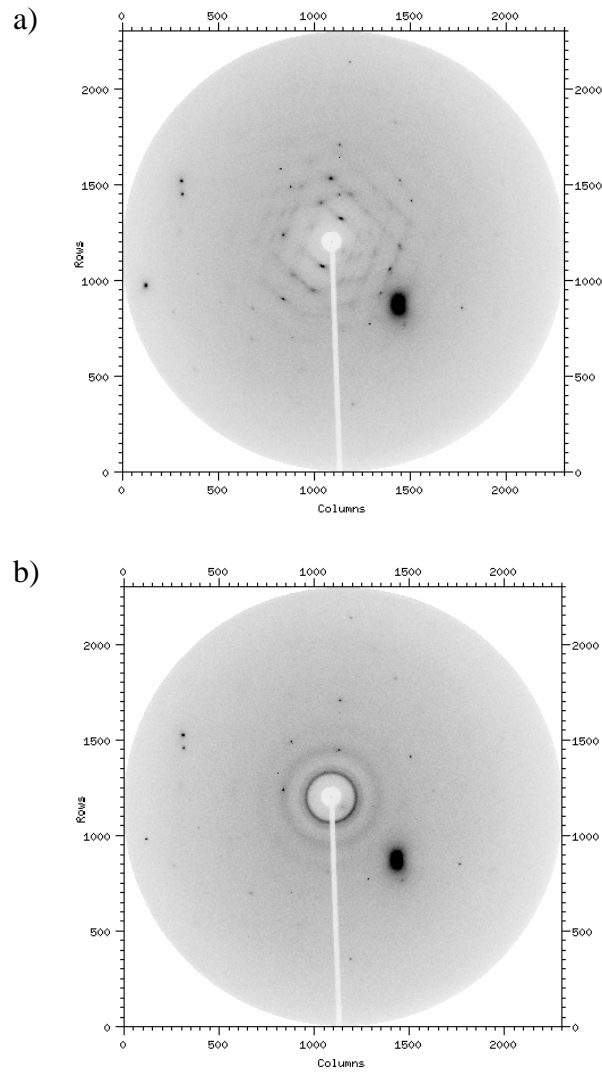
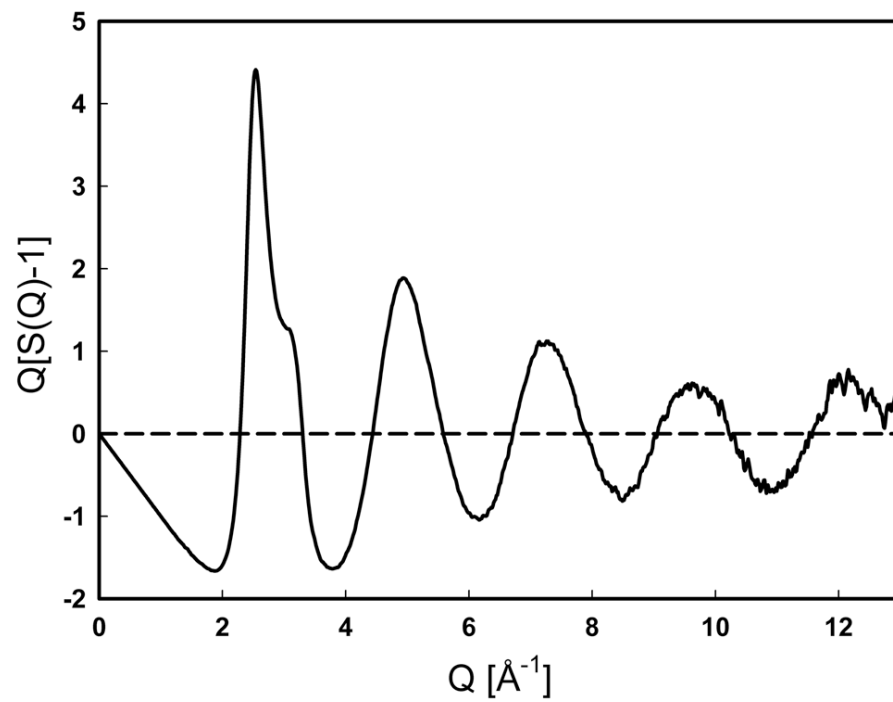


Figure 3.4 shows the collected total x-ray scattering patterns of a recrystallized solid phase gallium (Figure 3.4a) and a liquid phase gallium (Figure 3.4b). The characteristic diffraction spots of the solid phase gallium are not observed after reaching the melting point.



Ehm *et al.*, 2007

Figure 3.5 The normalized $S(Q)$.

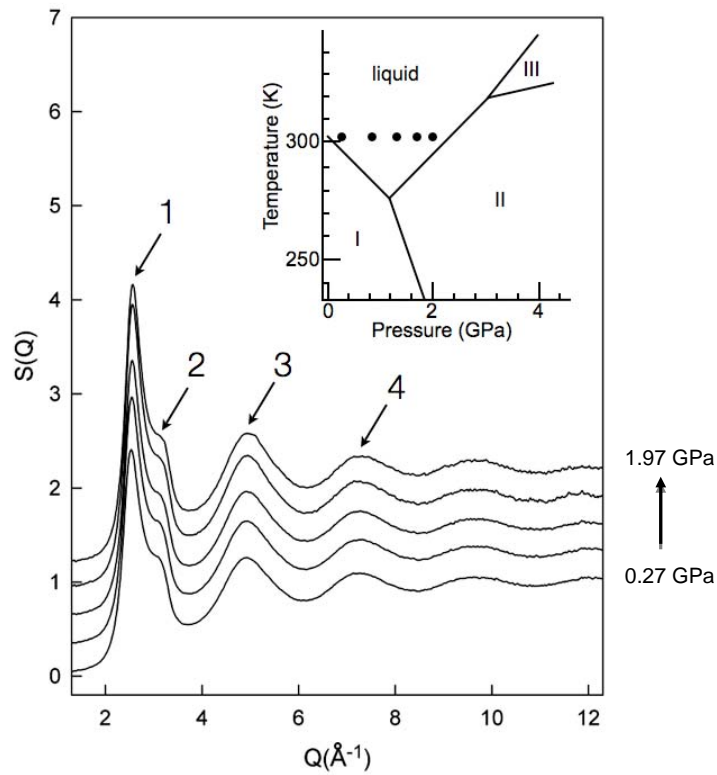


Figure 3.6 From the structure factor of liquid gallium, we see four maximums extending up to $Q=12 \text{ \AA}^{-1}$ from the total elastic scattering by the high energy ($\sim 80\text{KeV}$) synchrotron x-ray. The phase diagram of gallium (Bosio, 1978) shows that the liquid phase exists within the pressure range of 0.1GPa and 2GPa at room temperature. The solid circles show the pressure and temperature condition of the data points acquired for this experiment.

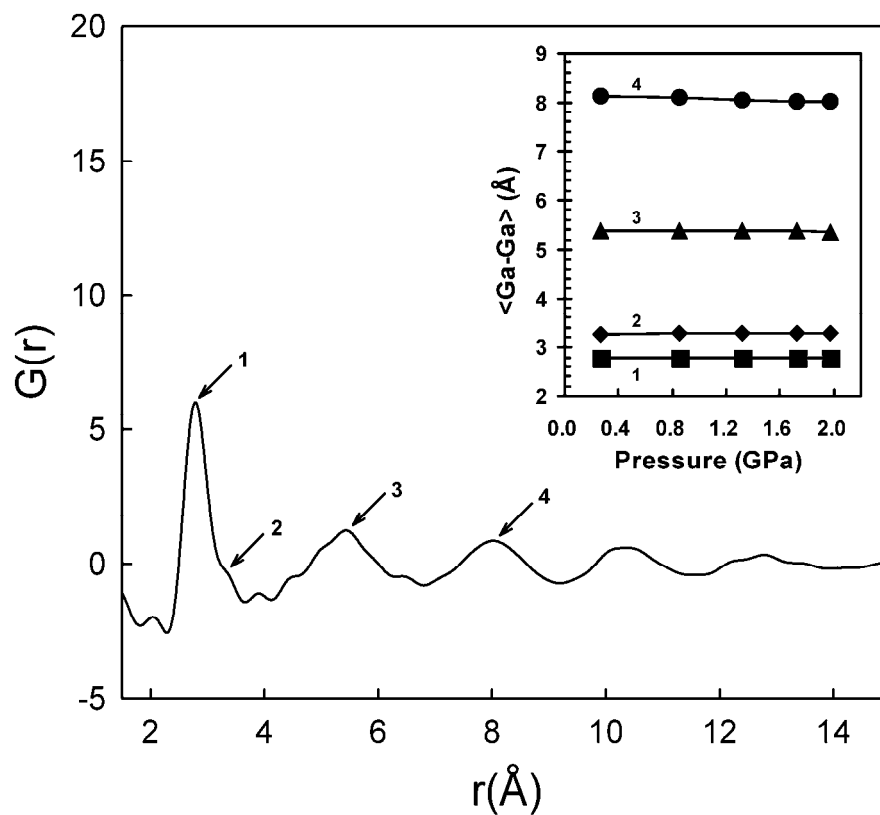


Figure 3.7 The PDF is obtained from the total scattering data via a sine Fourier transform of the normalized scattering intensity $S(Q)$. Therefore, the $G(r)$ shows atomic structure information in real space. The first large peak and its shoulder at 2.78 Å (#1) and 3.25 Å (#2) represent the distorted local dense-packed rigid unit. The tail accounts for the intermediate-range correlations. The inset illustrates the peak positions change with pressure. Peak #1 and #2 did not change with pressure but the third peak position decreased by an amount of 0.6%, and the fourth peak position decreased 1.5% with pressure increasing. This phenomenon is unusual for compression of hard spheres.

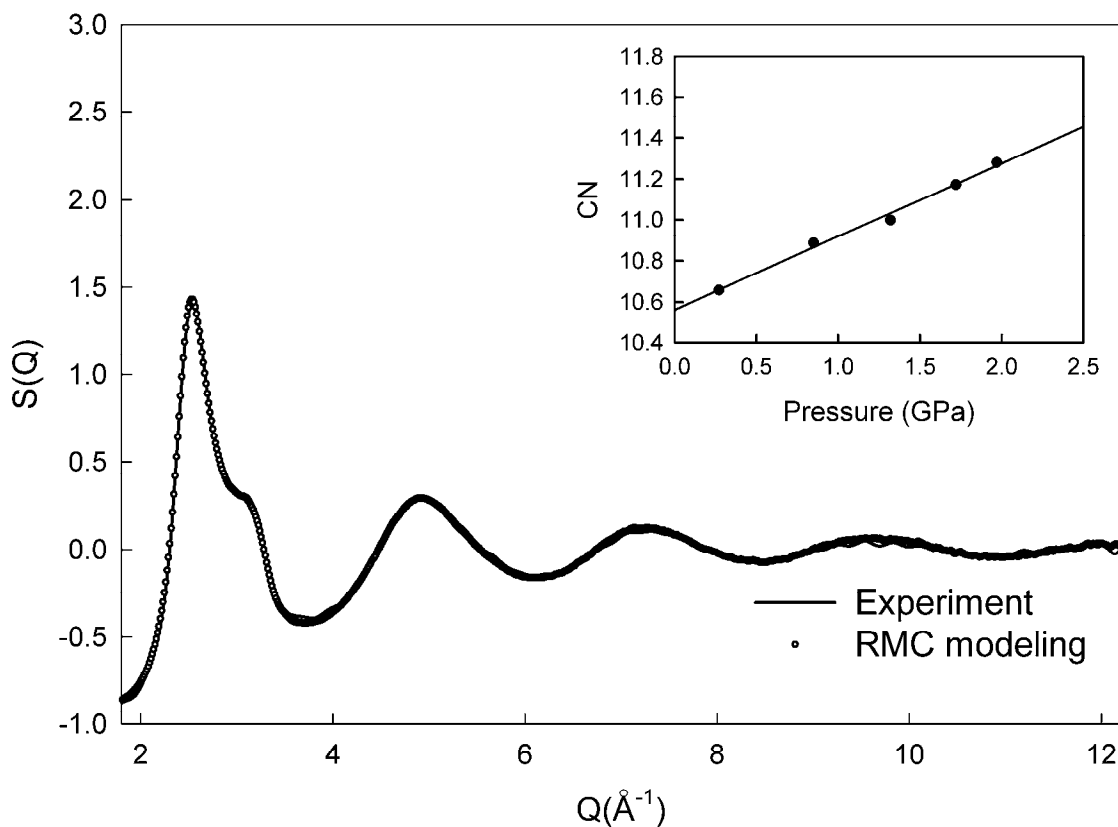


Figure 3.8 The Reverse Monte Carlo modeling result of the experimentally observed $S(Q)$ at 0.27GPa. The total number of atoms applied in the modeling process is 5000. The Reverse Monte Carlo modeling result (open circles) agrees well with the experimental observation (solid line). The coordination number linearly increases with pressure. This reflects the reduction of the distortion of the locally ordered unit.

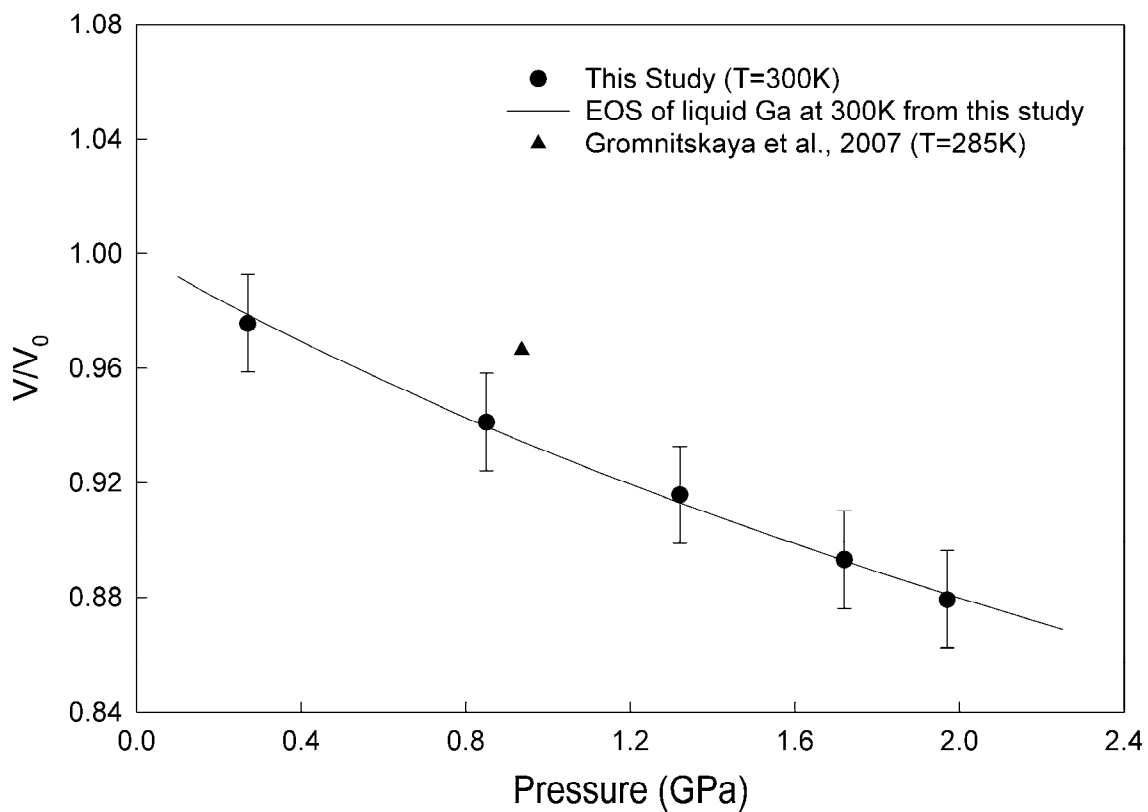


Figure 3.9 Shown is the fitted 2nd order Birch-Murnaghan equation of state volume compression curve of liquid gallium derived from the RMC modeling result. The calculated isothermal bulk modulus at 300K is 12.1(6) GPa for liquid gallium. For comparison, the triangle shape single data point result is graphically picked from previous ultrasonic measurements study of liquid gallium by Gromnitskaya *et al.* [2007].

Exploration for future work and summary

4.1 Exploration For Future Work

4.1.1 FeS Density Measurement

The accurate densities of liquid phase iron alloys are demanding for understanding the outer core. The experimental pressure range for melt density measurement in a large volume multi-anvil press is technically limited (in-situ ~10 GPa, ex-situ ~20GPa). Large extrapolations (to 130~330GPa) are needed in order to apply the equation of state results to the core condition. Even a small data uncertainty within the experimental pressure range will result in significant error in such a large extrapolation. Extending the pressure range for in situ liquid density measurements is essential for ultimately resolving the core composition issue. Therefore the immediate future work is

study melt density of Fe-S system at high pressure. Measuring liquid material density using a diamond anvil cell was first explored by Shen *et al.* (2001). Our preliminary experiments of measuring FeS liquid density in a diamond anvil cell have been performed at the Advanced Light Source. The high temperature was provided by a laser heating system. Figure 4.1 shows the image of the sample setup in the diamond anvil cell under a microscope. The x-ray absorption image of the sample is also shown. Two holes were drilled on the same gasket, each 120 μm in diameter. One hole was filled with fine Al_2O_3 powder as a sample thickness measurement. The other hole included FeS sample surrounded by fine Al_2O_3 powder. Thin layers of Al_2O_3 powder were loaded between the diamond anvil culets and the sample for thermal insulation. This experiment setup has potential to produce high pressure liquid density data. However, there do exist experimental details that need to be addressed. One of them is the determination of the sample thickness between the top and bottom thermal insulation layers. One way to minimize the thickness error is by coating the diamond culets with hard MgO or Al_2O_3 layers which have been proved effective (Andraut and Fiquet, 2001). Figure 4.2 shows the size comparison of the two sample holes at ambient pressure and under high pressure. The hole that contained the sample was not densely packed as the pure Al_2O_3 powder hole. Therefore, the diameter of the sample hole becomes smaller under pressure. A 4GPa difference in pressure between the two chambers was observed by the ruby scale at about 7.1GPa sample pressure. Continuation of technical development in this area is needed.

Even within the current large volume pressure range, more experimental data on Fe-Xwt%S system with a finer sulfur content variation, e.g. at 5wt%S step, are needed to minimize the uncertainty in the sulfur content influence on bulk modulus. Exploring influence of other light elements (e.g. C, H, O, Si) using the technique we have developed in large volume press is another future work for a better understanding of the composition of Earth's core.

4.1.2 Structural Study

In addition to the large data stretching in the pressure extrapolation, another significant error in the melt density at the core conditions may come from possible pressure-induced local structural change in the Fe-S system. Variation of local atomic arrangement may alter the bulk modulus i.e. equation of state of the system. Our ultimate goal of PDF study is to investigate influence of pressure on the short-range ordering in liquid Fe-S system. In addition to ambient temperature pair distribution function study of liquid gallium, high pressure and high temperature x-ray total scattering data of liquid gallium has been collected up to 200°C (Figure 4.3). The high temperature $G(r)$ s show similar major features as observed at ambient temperature (Figure 4.4). However the data quality of $G(r)$ at 100°C is poor. We looked at the $G(r)$'s 4 major peak positions and their changes with pressure at different temperature conditions (Figure 4.5). The position of Peak #1 remains unchanged at ambient temperature, 100°C, and 200°C. Peak #3 and #4 decrease with pressure. Peak #2 increases at 100°C but decreases at 200°C, showing an

inconsistent position change between different temperature conditions. Reason is unclear, but possibly due to the large error that was generated from the poor quality $G(r)$ at 100°C. Further investigation is needed. The calculated interatomic distance change with temperature at 1GPa and 4GPa is illustrated in Figure 4.6. Except Peak #2, the 3 other interatomic distances are not affected by temperature within the 200°C temperature range. Temperature seems to have a stronger effect on peak positions at lower pressure.

Although the temperatures we reached in these experiments are far below the melting temperature of FeS, we have gained experience on high temperature diffuse scattering data collection and processing. The future work in this area is to establish an experimental routine for PDF study using laser heated DAC, and to study pressure influence on local structure of Fe-S melt system. Bright synchrotron x-rays at Advanced Photon Source may be required for such experiments.

4.2 Summary

Density measurement of liquid phase FeS under high pressure and high temperature has been performed using radiography technique combined with x-ray synchrotron. The absorption image analyzed by our self-developed program provides reliable density results. The -1.8GPa/wt% bulk modulus versus sulfur content relationship proposed by our study is different from previous studies (Sanloup *et al.*, 2000). If 10wt% sulfur is responsible for the density deficit between pure iron and the liquid outer core,

the impact of these two trends will differ the sulfur content of the liquid outer core by 3wt%. More detailed density measurements and equation of state studies of different Fe-Xwt%S alloys are required to further confirm the trend.

In order to understand liquid density change with pressure and temperature, it is important to look at the liquid structure. In chapter 3, the atomic structure of a simple composition liquid --- gallium was investigated up to 12Å. This study helps us understand liquid structure with simple composition and its behavior under pressure. Most liquid gallium structure studies were limited at the first nearest neighbor. We have extended the atomic structure study beyond this range. The technique could be applied to multi-element materials and our ultimate goal is to study the liquid structure of earth materials. Since earth materials are generally complicated in composition, the investigation of the atomic structure of a simple element does shed light on an experimental procedure to detect multi-element liquid structure farther than the first nearest neighbor distance.

Almost all the experiments that have contributed to this dissertation were performed at the National Synchrotron Light Source at the Brookhaven National Laboratory. Nowadays, many high pressure and high temperature mineral physics experiments and studies of the interior of the earth strongly benefit and rely on synchrotron x-ray. Future study direction will keep taking advantage of the light sources, and focus on applying synchrotron x-ray to earth related materials in order to help us better understand our planet.

4.3 References

- Andrault, D., G. Fiquet, 2001, Synchrotron radiation and laser heating in a diamond anvil cell, *Review of Scientific Instruments*, 72, 1283-1288.
- Comez, L., A. Di Cicco, J. P. Itie, A. Polian, 2001, High-pressure and high-temperature x-ray absorption study of liquid and solid gallium, *Physical Review B*, 65, 014114.
- Sanloup, C., F. Guyot, P. Gillet, G. Fiquet, M. Mezouar, I. Martinez, 2000, Density measurements of liquid Fe-S alloys at high-pressure, *Geophysical Research Letters*, 27(6), 811-814.
- Shen, G. Y., N. Sata, M. L. Rivers, and S. R. Sutton, 2001, Melting of indium at high pressure determined by monochromatic x-ray diffraction in an externally-heated diamond anvil cell, *Applied Physics Letters*, 78(21), 3208-3210.

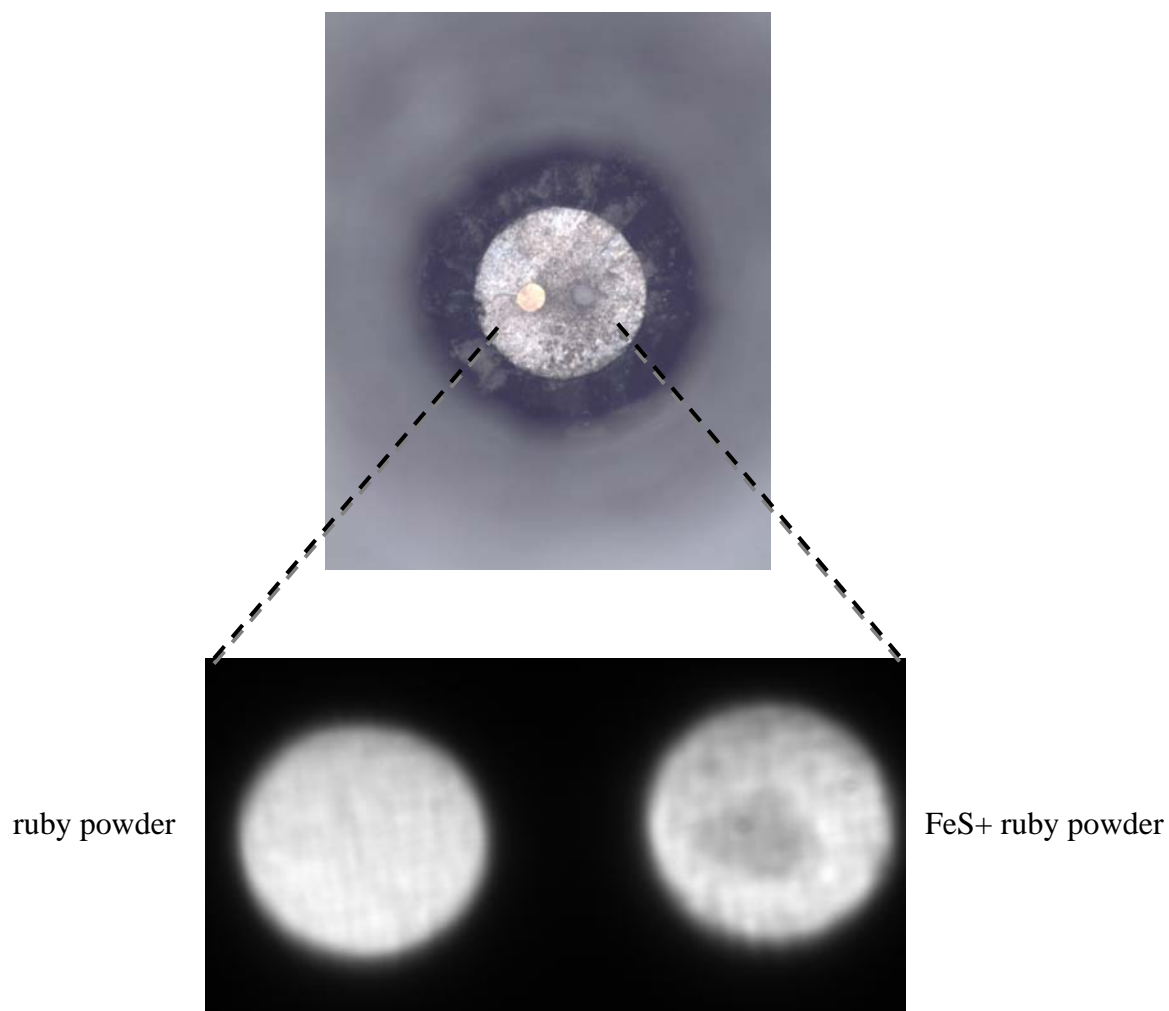


Figure 4.1 shows the image of the gasket and the samples in the diamond anvil cell. Two holes were drilled on the same gasket, each 120 μm in diameter. The left hole was filled with fine Al_2O_3 powder as a sample thickness measurement. The other hole included FeS sample (darker part) surrounded by fine Al_2O_3 powder.

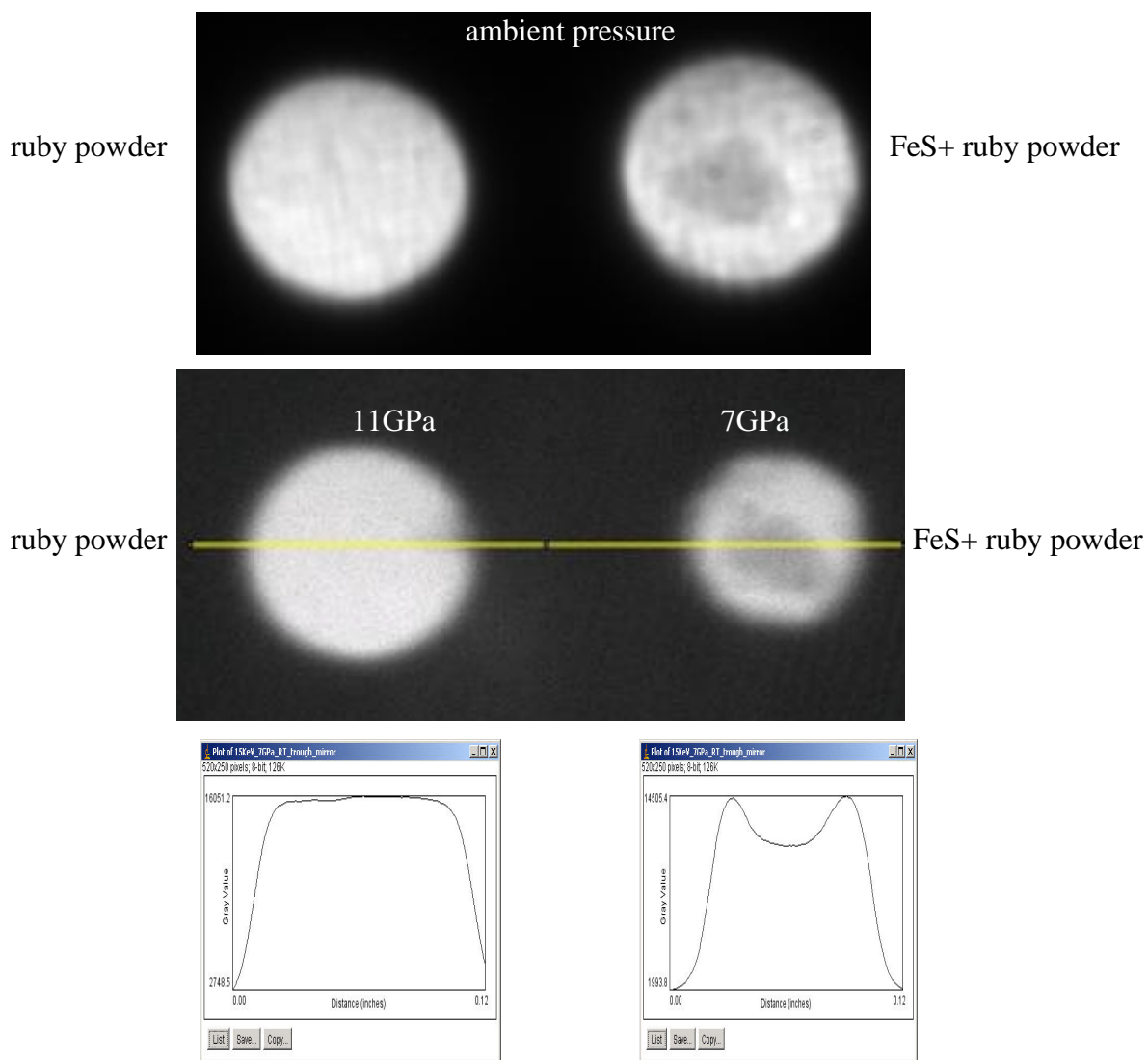


Figure 4.2 The size comparison of the two gasket holes at ambient pressure and under high pressure. The hole that contains the sample (right hand side) was not densely packed as the pure Al_2O_3 powder hole (left hand side). Therefore, the diameter of the sample hole becomes smaller under pressure. A 4GPa difference in pressure between the two chambers was observed by the ruby scale. The x-ray absorption intensity profile along the yellow line is shown at the very bottom.

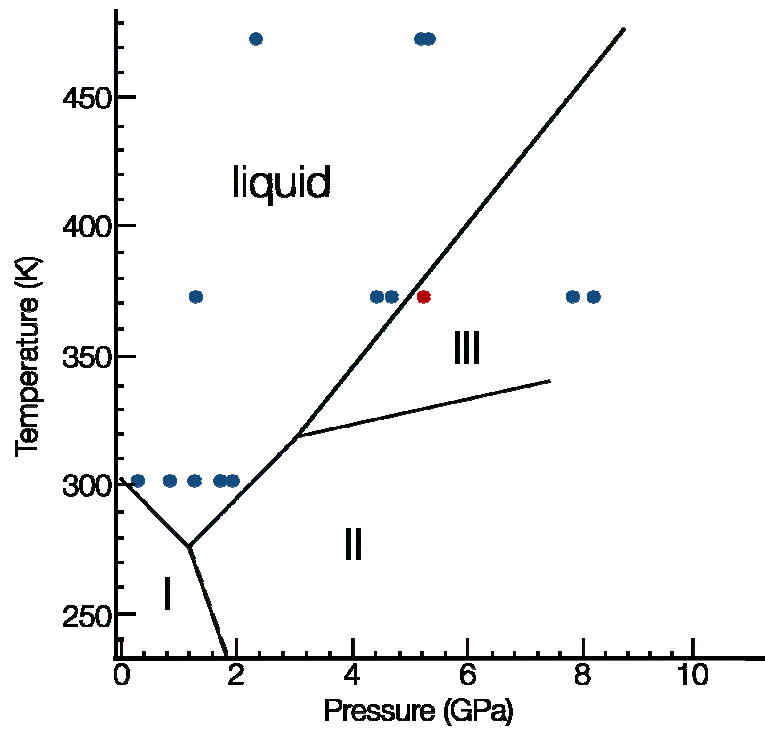


Figure 4.3 High pressure and high temperature x-ray total scattering data of liquid gallium has been collected up to 200°C.

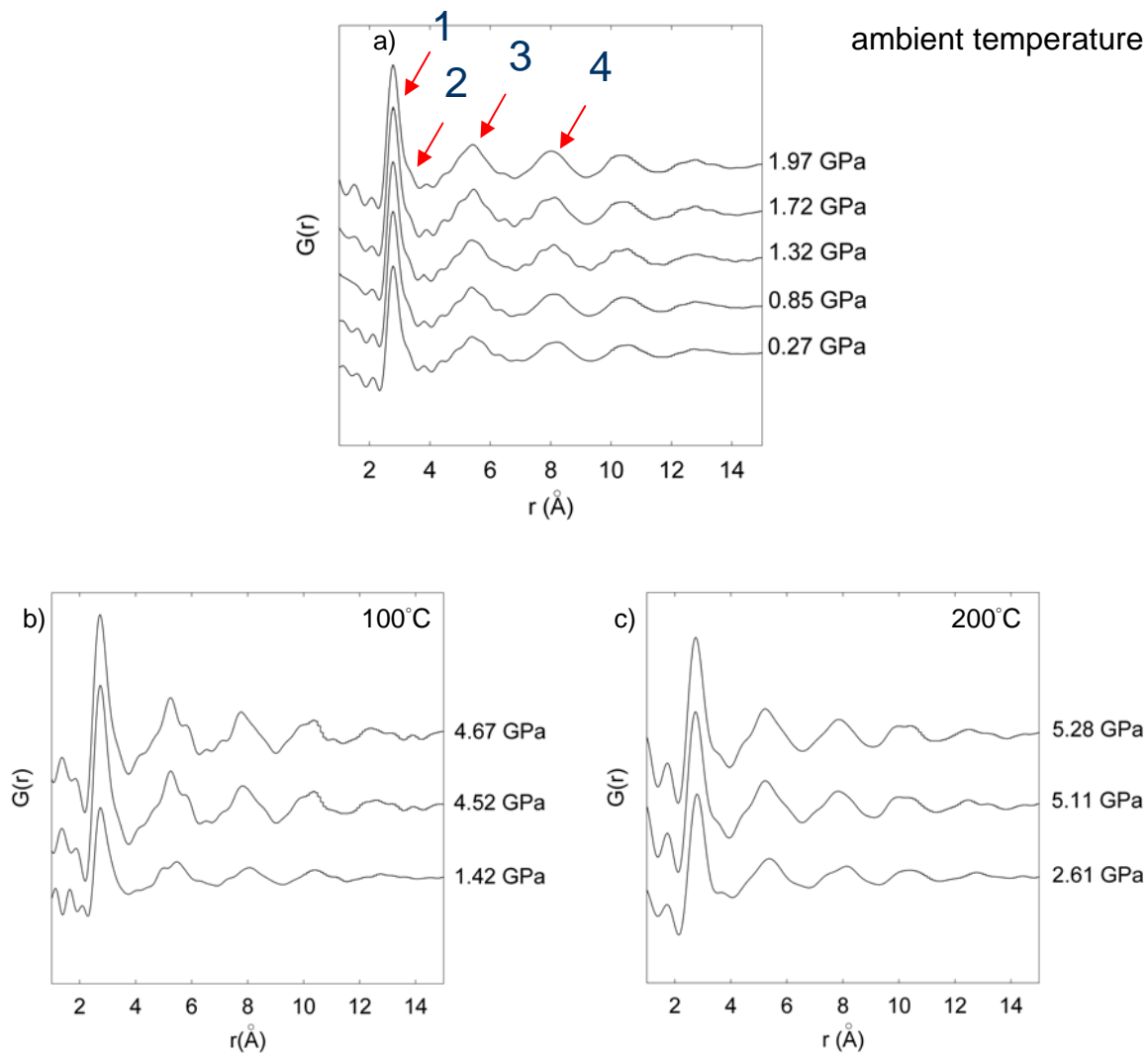


Figure 4.4 This figure shows the final PDF $G(r)$ results of liquid gallium collected at ambient temperature (**Figure 4.4a**), 100°C (**Figure 4.4b**), and 200°C (**Figure 4.4c**) at various pressure conditions up to 5.28GPa. The broad but distinctive peaks show where the near-neighbor atoms are located in the local atomic structure. The tail accounts for the medium and long-range correlations. The high temperature $G(r)$ s show similar major features as observed at ambient temperature.

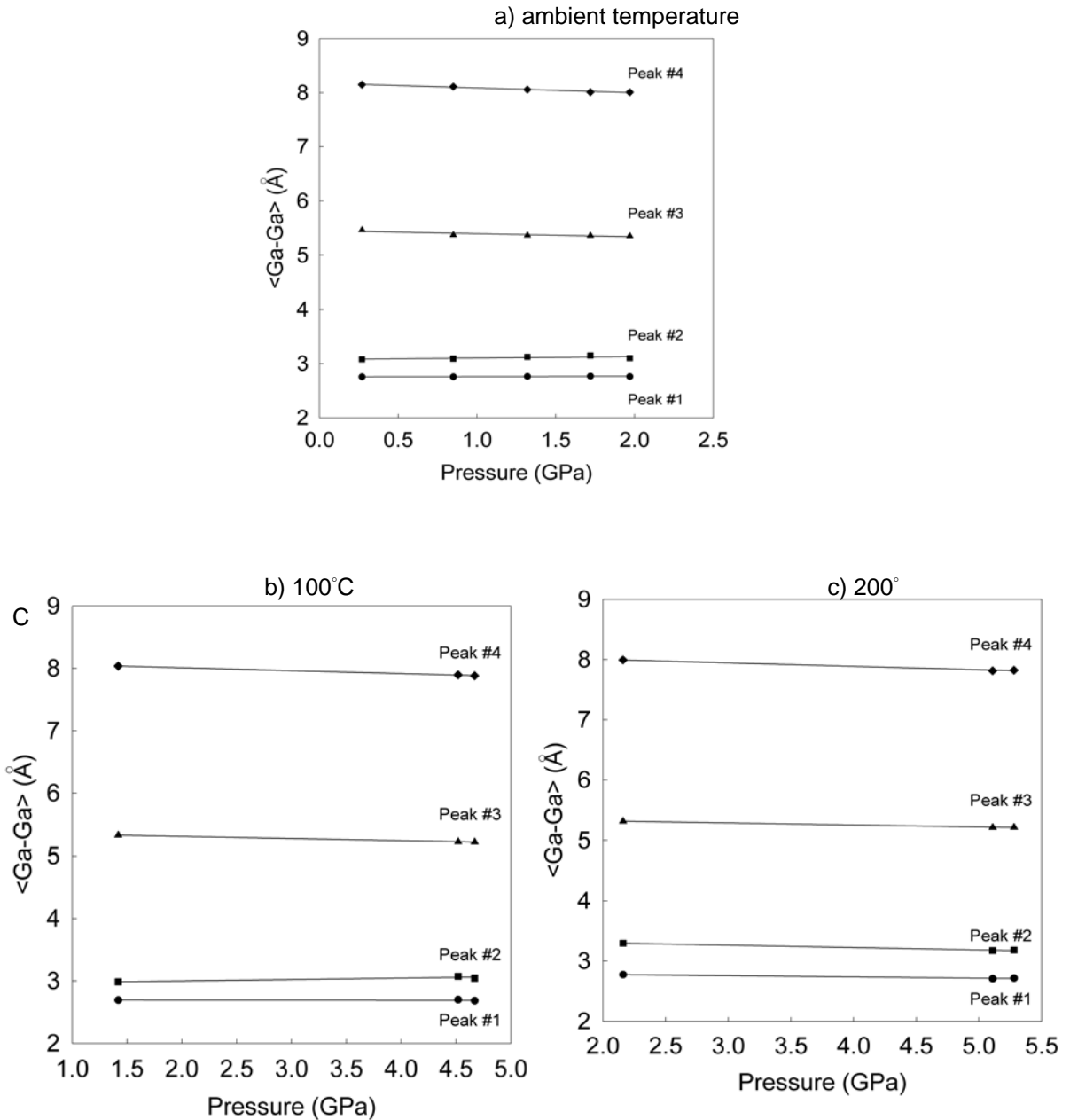
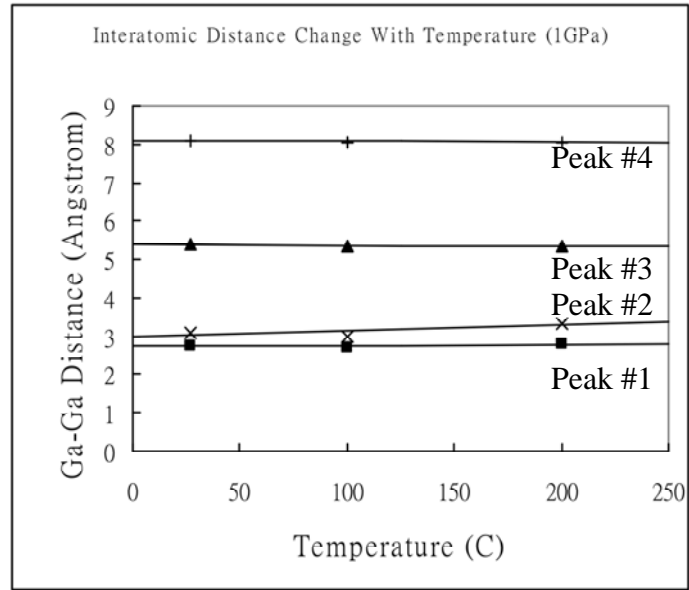


Figure 4.5 The position of Peak #1 remains unchanged at ambient temperature (**Figure 4.5a**), 100°C (**Figure 4.5b**), and 200°C (**Figure 4.5c**). Peak #3 and #4 decrease with pressure. Peak #2 increases at 100°C but decreases at 200°C, showing an inconsistent position change between different temperature conditions. Reason is unclear, but possibly due to the large error that was generated from the poor quality $G(r)$ at 100°C. Further investigation is needed.

a) 1GPa



b) 4GPa

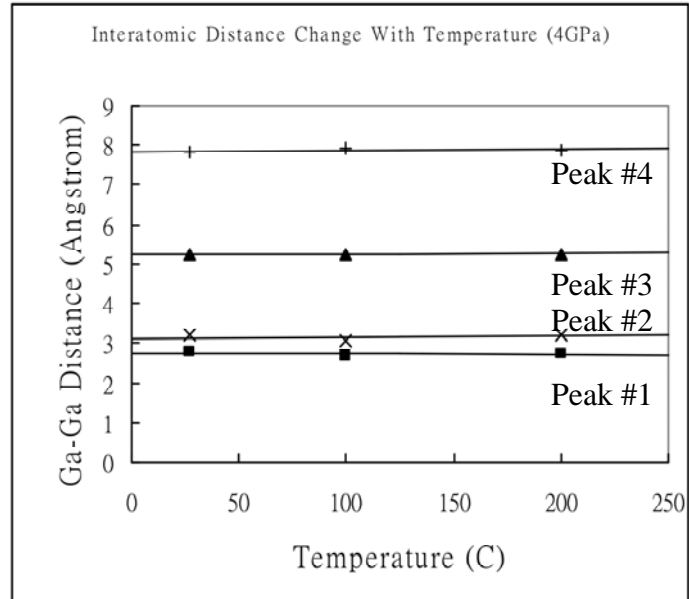


Figure 4.6 The calculated interatomic distance change with temperature at 1GPa and 4GPa. Except Peak #2, the 3 other interatomic distances are not affected by temperature within the 200°C temperature range. Temperature has a stronger effect on peak position change at 1GPa.

References

Chapter 1

- Ahrens, T. J., 1979, Equations of state of iron sulfide and constraints on the sulfur content of the Earth, *Journal of Geophysical Research*, 84(B3), 985-998. rhhotite and the Earth's core, *Journal of Geophysical Research*, 89, 6041-6048.
- Ahrens, T. J. and R. Jeanloz, 1987, Pyrite: shock compression, isentropic release, and composition of the Earth's core, *Journal of Geophysical Research, B, Solid Earth and Planets*, 92(10), 10,363-10,375.
- Balog, P. S., R. A. Secco, D. C. Rubie, and D. J. Frost, 2003, Equation of state of liquid Fe-10wt%S: Implications for the metallic cores of planetary bodies, *Journal of Geophysical Research*, 108, B2, 2124, ECV 11-1-ECV 11-11.
- Birch, F., 1952, Elasticity and constitution of the Earth's interior, *Journal of Geophysical Research*, 57(2), 227-286.
- Birch, F., 1964, Density and composition of mantle and core, *Journal of Geophysical Research*, 69(20), 4377-4388.
- Brett, R., 1984, Chemical equilibration of the Earth's core and upper mantle, *Geochimica et Cosmochimica Acta*, 48(6), 1183-1188.
- Brown, J. M., T. J. Ahrens, and D. L. Shampine, 1984, Hugoniot data for pyrrhotite and the Earth's core, *Journal of Geophysical Research*, 89, 6041-6048.
- Chen, J., D. J. Weidner, L. Wang, M. T. Vaughan, and C. E. Young, 2005, Density measurements of molten materials at high pressure using synchrotron x-ray

- radiography: Melting volume of FeS, in *Advances in High-Pressure Technology for Geophysical Applications*, Eds. J. Chen, Y. Wang, T.S. Duffy, G. Shen and L.F. Dobrzhinetskaya, ELSEVIER, Amsterdam, pp. 185-194.
- Dziewonski, A., and D. Anderson, 1981, Preliminary reference Earth model, *Physics of the Earth and Planetary Interiors*, 25, 297-356.
- Ganapathy, R. and E. Anders, 1974, Bulk compositions of the Moon and Earth, estimated from meteorites, *Lunar Science V*, Abstracts, Lunar Sci. Inst., Houston, Texas, 254-256.
- Hillgren, V. J., C. K. Gessmann, and J. Li, 2000, An experimental perspective on the light element in Earth's core. In *Origin of the Earth and Moon* (eds. R. M. Canup and K. Righter), 245-263. The University of Arizona Press, Tucson.
- Jeanloz, R., 1979, Properties of iron at high pressures and the state of the core, *Journal of Geophysical Research*, 84(NB11), 6059-6069.
- McGreevy R.L., 2001, Reverse Monte Carlo modeling, *J. Phys. Condens. Matter*, 13, 46, R877-R913.
- McDonough, W. F., 2003, in *Treatise on Geochemistry*, ed Carlson R.W., Elsevier, New York, 2, 547-568.
- McQueen, R. G., and S. P. Marsh, 1966, Shock-wave compression of iron-nickel alloys and the Earth's core, *Journal of Geophysical Research*, 71, 1751-1756.

- Morard, G., C. Sanloup, G. Fiquet, M. Mezouar, N. Rey, R. Poloni, P. Beck, 2007, Structure of eutectic Fe-FeS melts to pressures up to 17 GPa: Implications for planetary cores, *Earth and Planetary Science Letters*, 263, 128-139.
- Nishida, K., H. Terasaki, E. Ohtani, A. Suzuki, 2008, The effect of sulfur content on density of the liquid Fe-S at high pressure, *Phys. Chem. Minerals*, 35, 417-423.
- Poirier, J. P., 1994, Light elements in the Earth's outer core- a critical- review, *Physics of the Earth and Planetary Interiors*, 85 (3-4), 319-337.
- Sanloup, C., F. Guyot, P. Gillet, G. Fiquet, M. Mezouar, I. Martinez, 2000, Density measurements of liquid Fe-S alloys at high-pressure, *Geophysical Research Letters*, 27(6), 811-814.
- Secco, R. A., M. D. Rutter, P. S. Balog, H. Liu, D. C. Rubie, T. Uchida, D. Frost, Y. Wang, M. Rivers, S. R. Sutton, 2002, Viscosity and density of Fe-S liquids at high pressures, *J. Phys. Condens. Matter*, 14, 11325-11330.

Chapter 2

- Ahrens, T. J., 1979, Equations of state of iron sulfide and constraints on the sulfur content of the Earth, *Journal of Geophysical Research*, 84(B3), 985-998.
- Ahrens, T. J. and R. Jeanloz, 1987, Pyrite: shock compression, isentropic release, and composition of the Earth's core, *Journal of Geophysical Research, B, Solid Earth and Planets*, 92(10), 10,363-10,375.

- Angel, R. J., 2000, Equations of state, *High temperature and high pressure crystal chemistry. Reviews in mineralogy and geochemistry*, 41, 35-59.
- Balog, P. S., R. A. Secco, D. C. Rubie, and D. J. Frost, 2003, Equation of state of liquid Fe-10wt%S: Implications for the metallic cores of planetary bodies, *Journal of Geophysical Research*, 108, B2, 2124, ECV 11-1-ECV 11-11.
- Birch, F., 1952, Elasticity and constitution of the Earth's interior, *Journal of Geophysical Research*, 57(2), 227-286.
- Birch, F., 1964, Density and composition of mantle and core, *Journal of Geophysical Research*, 69(20), 4377-4388.
- Brett, R., 1984, Chemical equilibration of the Earth's core and upper mantle, *Geochimica et Cosmochimica Acta*, 48(6), 1183-1188.
- Brown, J. M., T. J. Ahrens, and D. L. Shampine, 1984, Hugoniot data for pyrrhotite and the Earth's core, *Journal of Geophysical Research*, 89, 6041-6048.
- Chen, J., D. J. Weidner, L. Wang, M. T. Vaughan, and C. E. Young, 2005, Density measurements of molten materials at high pressure using synchrotron x-ray radiography: Melting volume of FeS, in *Advances in High-Pressure Technology for Geophysical Applications*, Eds. J. Chen, Y. Wang, T.S. Duffy, G. Shen and L.F. Dobrzhinetskaya, ELSEVIER, Amsterdam, pp. 185-194.
- Compton, A. H. and S. K. Allison, 1935, *X-Rays in Theory and Experiment*, D. Van Nostrand Company, INC., London, pp. 828.

- Decker, D. L., 1971, High-pressure equation of state for NaCl, KCl and CsCl, *Journal of Applied Physics*, 42, 3239-3244.
- Fei, Y. W., C. T. Prewitt, H. K. Mao, and C. M. Bertka, 1995, Structure and Density of FeS at High Pressure and High Temperature and the Internal Structure of Mars, *Science*, 268(5219), 1892-1894.
- Ganapathy, R. and E. Anders, 1974, Bulk compositions of the Moon and Earth, estimated from meteorites, *Lunar Science V*, Abstracts, Lunar Sci. Inst., Houston, Texas, 254-256.
- Henke, B. L., E. M. Gullikson, and J. C. Davis, 1993, X-ray interactions: photoabsorption, scattering, transmission, and reflection at E= 50-30,000 eV, Z=1-92, *Atomic Data and Nuclear Data Tables*, 54, 181-342.
- Hillgren, V. J., C. K. Gessmann, and J. Li, 2000, An experimental perspective on the light element in Earth's core. In *Origin of the Earth and Moon* (eds. R. M. Canup and K. Righter), 245-263. The University of Arizona Press, Tucson.
- Hixson, R. S., M. A. Winkler, M. L. Hodgon, 1990, Sound speed and thermophysical properties of liquid iron and nickel, *Phys. Rev. B*, 42, 6485-6491.
- Jeanloz, R., 1979, Properties of iron at high pressures and the state of the core, *Journal of Geophysical Research*, 84(NB11), 6059-6069.
- Li, J. and Y. W. Fei, 2003, Experimental constraints on core composition, *Geochemistry of the Mantle and Core* (ed. R. W. Carlson), 521-546

- McQueen, R. G., and S. P. Marsh, 1966, Shock-wave compression of iron-nickel alloys and the Earth's core, *Journal of Geophysical Research*, 71, 1751-1756.
- Nagamori, M., 1969, Density of molten Ag-S, Cu-S, and Ni-S systems, *Trans. Metall. Soc. AIME* 245, 1897-1902.
- Nishida, K., H. Terasaki, E. Ohtani, A. Suzuki, 2008, The effect of sulfur content on density of the liquid Fe-S at high pressure, *Phys. Chem. Minerals*, 35, 417-423.
- Poirier, J. P., 1994, Light elements in the Earth's outer core- a critical- review, *Physics of the Earth and Planetary Interiors*, 85 (3-4), 319-337.
- Sanloup, C., F. Guyot, P. Gillet, G. Fiquet, M. Mezouar, I. Martinez, 2000, Density measurements of liquid Fe-S alloys at high-pressure, *Geophysical Research Letters*, 27(6), 811-814.
- Secco, R. A., M. D. Rutter, S. P. Balog, H. Liu, D. C. Rubie, T. Uchida, D. Frost, Y. Wang, M. Rivers, and S. R. Sutton, 2002, Viscosity and density of Fe-S liquids at high pressures, *Journal of Physics: Condensed Matter*, 14, 11325-11330.
- Tsuchiya, Y., 1994, The thermodynamics of structural changes in the liquid sulfur-tellurium system: compressibility and Ehrenfest's relations, *Journal of Physics: Condensed Matter*, 6, 2451-2458.

Chapter 3

- Bosio, L., 1978, Crystal structures of Ga(II) and Ga(III), *J. Chem. Phys.*, 68, 1221-1223.
- Brazhkin, V. V., S. V. Popova, R. N. Voloshin, 1997, High-pressure transformations in simple melts, *High Pressure Research*, 15, 267-305.

- Brown, Jr., G. E., F. Farges, G. Calas, 1995, X-ray scattering and x-ray spectroscopy studies of silicate melts, *Reviews in Mineralogy*, 32, 317-410.
- Comez, L., A. Di Cicco, J. P. Itie, and A. Polian, 2001, High-pressure and high-temperature x-ray absorption study of liquid and solid gallium, *Physical Review B*, 65, 014114-1-014114-10.
- Comez, L., A. Di Cicco, M. Minicucci, R. Tossici, J. P. Itie, and A. Polian, 2001, EXAFS study on liquid gallium under high pressure and high temperature, *J. Synchrotron Rad.*, 8, 776-778.
- Di Cicco, A. and A. Filipponi, 1993, Three-body distribution function in liquids: the case of liquid gallium, *J. Non-Cryst. Sol.*, 156-158, 102-106.
- Ehm, L., S. M. Antao, J. Chen, D. R. Locke, F. M. Michel, C. D. Martin, T. Yu, J. B. Parise, P. L. Lee, P. J. Chupas, S. D. Shastri, Q. Guo, 2007, Studies of local and intermediate range structure in crystalline and amorphous materials at high pressure using high-energy x-rays, *Powder Diffraction*, 22 (2), 108-112.
- Funamuri, N., K. Tsuji, 2002, Pressure induced structural change in liquid silicon, *Physical Review Letters*, 88(25), 255508-1-255508-4.
- Funamuri, N., K. Tsuji, 2002, Structural transformation of liquid tellurium at high pressures and temperatures, *Physical Review B*, 65(1), 014105-1-014105-5.
- Glosli, J. N., F. H. Ree, 1999, Liquid-liquid phase transformation in carbon, *Physical Review Letters*, 82 (23), 4659-4662.

- Gromnitskaya, E.L., O. F. Yagafarov, O. V. Stagorova, V. V. Brazhkin, A. G. Lyapin, 2007, Pressure-driven “molecular metal” to “atomic metal” transition in crystalline Ga, *Physical Review Letters*, 98, 165503.
- Hammersley, A. P., S. O. Svensson, M. Hanfland, A. N. Fitch, D. Hausermann, 1996, Two-dimensional detector software: From real detector to idealized image or two-theta scan, *High Pressure Research*, 14, 235-248.
- Hammersley, A. P., 1997, FIT2D: An introduction and overview, *ESRF Internal Report*, ESRF97HA02T.
- Hoather, W. H., 1936, The density and coefficient of expansion of liquid gallium over a wide range of temperature, *Proceedings of the Physical Society*, 48, 5, 699-707.
- Hui, L., G. Wang, J. Zhao, X. Bian, 2002, Cluster structure and dynamics of liquid aluminum under cooling conditions, *J. Chem. Phys.*, 116, 10809-10815.
- Katayama, Y., K. Tsuji, H. Kanda, H. Nosaka, K. Yaoita, T. Kikegawa, O. Shimomura, 1996, Density of liquid tellurium under pressure, *Journal of Non-crystalline Solids*, 207, 451-454.
- Katayama, Y., T. Mizutani, W. Utsumi, O. Shimomura, M. Yamakata, K. Funakoshi, 2000, A first-order liquid-liquid phase transition in phosphorus, *Nature*, 403(6766), 170-173.
- Katayama, Y., T. Mizutani, W. Utsumi, O. Shimomura, K. Tsuji, 2001, X-ray diffraction study on structural change in liquid selenium under high pressure, *Physica Status Solidi (b)*, 223, 401-404.

- Katayama, Y., Y. Inamura, 2003, Synchrotron radiation studies on pressure-induced structural changes in liquids and glasses, *Journal of Physics: Condensed Matter*, 15(1), S343-S350.
- Katayama, Y., K. Tsuji, 2003, X-ray structural studies on elemental liquids under high pressures, *Journal of Physics: Condensed Matter*, 15, 23, 6085-6103.
- McGreevy, R.L., 2001, Reverse Monte Carlo modeling, *Journal of Physics: Condensed Matter*, 13, 46, R877-R913.
- Parise, J. B., S. M. Antao, F. M. Michel, C. D. Martin, P. J. Chupas, S. D. Shastri, and P. L. Lee, 2005, Quantitative high-pressure pair distribution function analysis, *J. Synchrotron Rad.*, 12, 554-559.
- Proffen, Th. and S. J. L. Billinge, 1999, PDFFIT, a program for full profile structural refinement of the atomic pair distribution function, *J. Appl. Cryst.*, 32, 572-575.
- Qiu, X., J. W. Thompson, and S. J. L. Billinge, 2004, PDFgetX2: A GUI driven program to obtain the pair distribution function from X-ray powder diffraction data, *J. Appl. Cryst.*, 37, 678-678.
- Tanaka, H., 2000, General view of a liquid-liquid phase transition, *Physical Review E*, 62 (5), 6968-6976.
- Tsay, S. F., 1993, Structure of rapidly quenched Ga metal, *Phys. Rev. B*, 48, 5945-5948.
- Waseda, Y. and K. Suzuki, 1972, Structure factor and atomic distribution in liquid metals by x-ray diffraction, *Phys. Stat. Sol. B*, 49, 339-347.
- Waseda, Y., 1980, *The Structure of Non-Crystalline Materials*, New York, McGraw-Hill.

Wei, S., H. Oyanagi, W. Liu, T. Hu, S. Yin, G. Bian, 2000, Local structure of liquid gallium studied by x-ray absorption fine structure, *J. Non-Cryst. Sol.*, 275, 160-168.

Yaoita, K., K. Tsuji, M. Imai, T. Kikegawa, O. Shimomura, 1990, Structure of liquid bismuth under high pressure, *High Pressure Research*, 4 (1), 339-341.

Chapter 4

Andrault, D., G. Fiquet, 2001, Synchrotron radiation and laser heating in a diamond anvil cell, *Review of Scientific Instruments*, 72, 1283-1288.

Comez, L., A. Di Cicco, J. P. Itie, A. Polian, 2001, High-pressure and high-temperature x-ray absorption study of liquid and solid gallium, *Physical Review B*, 65, 014114.

Sanloup, C., F. Guyot, P. Gillet, G. Fiquet, M. Mezouar, I. Martinez, 2000, Density measurements of liquid Fe-S alloys at high-pressure, *Geophysical Research Letters*, 27(6), 811-814.

Shen, G. Y., N. Sata, M. L. Rivers, and S. R. Sutton, 2001, Melting of indium at high pressure determined by monochromatic x-ray diffraction in an externally-heated diamond anvil cell, *Applied Physics Letters*, 78(21), 3208-3210.